University of Nevada, Reno

How Future Hyperspectral Satellite Spectrometer Systems Can Improve Fractional Snow-covered Area and Grain Size

A thesis submitted in partial fulfillment of the
requirements for the degree of
Master of Science in Geophysics

by

Ryley G. Hill

Dr. Wendy Calvin, Thesis Advisor

May, 2018

UNIVERSITY OF NEVADA, RENO

THE GRADUATE SCHOOL

We recommend that the thesis

prepared under our supervision by

Ryley G. Hill

entitled

How Future Hyperspectral Satellite Spectrometer Systems Can Improve Fractional Snow-covered Area and Grain Size

be accepted in partial fulfillment of the

requirements for the degree of

MASTER OF SCIENCE

Wendy Calvin, Ph.D., Advisor

John Louie, Ph.D., Committee Member

Adrian Harpold, Ph.D., Graduate School Representative

David W. Zeh, Ph.D., Dean, Graduate School

May, 2018

Abstract

The impact of a declining and erratic seasonal mountain snowpack in North America and most of Eurasia may prove a detrimental hydrological, climatological, and environmental hazard as well as put a burden on those who rely on snow storage as their dominant source of water. There is a constant need to refine fractional snow-covered area (fSCA) and snow grain size calculations as they are a significant parameter in regional to global hydrological, ecological, and climate models. While the methods for determining fSCA and grain size are well understood for varying aerial and satellite multispectral imaging spectrometer (IS) systems, the improvements that a hyperspectral satellite IS system might bring to fSCA and grain size calculations is not well understood. As an analog for future IS systems, previously collected Airborne Visible/Infrared Imaging Spectrometer (AVIRIS) data serves the unique purpose of parameterizing the effects that future hyperspectral satellite IS systems will have on current fSCA and grain size retrieval algorithms. The following work explores the development of a fSCA and grain size retrieval model in order to understand how the differences in future hyperspectral satellite IS systems compare to current snow products. The open-source model will hopefully expand optimization and use to a variety of different IS systems and spectral unmixing tasks.

Life isn't about waiting for the storm to pass..

It's about learning to dance in the rain.

-Vivian Greene

Acknowledgements

I would first like to acknowledge the funding sources that allowed any of the previous acquisition of the data and subsequent work to exist. The AVIRIS data collection was provided in collaboration with a Nevada NASA EPSCoR project. Additionally, I would like to thank the pipeline processing and correction of the AVIRIS data that was supported under NASA HyspIRI Preparatory Airborne Activities Grant to the University of Nevada, Reno. I need to especially thank Dr. Wendy Calvin for providing funding for this work though her discretionary funds from the State of Nevada and her immense support as an outstanding mentor and friend who has inspired me to continue my research efforts even if they are not directly related to remote sensing. This project in particular would never have been initiated if it was not for Dr. Wendy Calvin taking me on as her student when previous circumstances looked ominous. I must also acknowledge Dr. Adrian Harpold who provided substantial feedback in the early stages of the thesis development that allowed for improved direction and purpose. I must also mention the continued support and patience of my long standing and outstanding mentor Dr. John Louie- from taking his classes, asking questions, and helping in his class he has always been there.

Lastly, I would like to thank all my friends and loved ones who have continued to support and grow with me in Reno these past two years. My best friend Eliza has helped me tackle all of my most difficult problems and I owe it nearly all to her that I'm so glad to have finally conquered them. The quote on the previous page is one of her favorites and remains an approach to life that we should all strive for.

Contents

Abstract **i**

Acknowledgements **iii**

List of Tables **v**

List of Figures **vi**

1 Introduction **1**

2 Algorithm Development **5**
2.1 Abstract . . . 5
2.2 Introduction . . . 5
2.2.1 Linear Spectral Mixture Analysis in Snow Science . . . 7
2.2.2 Preliminary Algorithm . . . 9
2.3 Model Description . . . 10
2.3.1 Development of Endmembers . . . 10
2.3.2 Development of Spectral Mixture Analysis . . . 16
2.4 Sensitivity Analysis . . . 17
2.5 Final Improvements . . . 18

3 Manuscript for submission to Remote Sensing of Environment; Title: Next Generation Snow Cover Mapping: How Future Hyperspectral Satellite Spectrometer Systems Can Improve Subpixel Snow-covered Area and Grain Size **24**
3.1 Abstract . . . 24
3.2 Introduction . . . 25
3.3 Background . . . 27
3.3.1 Snow Covered Area . . . 27
3.3.2 Snow Grain Size . . . 27
3.4 Data and Simulated Data . . . 29
3.4.1 AVIRIS Flights . . . 29
3.4.2 Current Snow Mapping Products . . . 29
3.4.3 Simulated MODSCAG, CASI, EnMAP, and beyond . . . 31
3.5 Model Description . . . 34
3.5.1 Library Endmembers . . . 34
3.5.2 Spectral Mixture Analysis . . . 35

3.6 Sensitivity Study 38
3.7 Comparisons 40
3.7.1 Comparison Metrics 41
3.7.2 Comparison Statistics 41
3.8 Discussion 52
3.9 Conclusion 56
3.10 Acknowledgements 58

A **59**

References **62**

List of Tables

3.1 MODIS Bands 30
3.2 Snow Mapping Products 32
3.3 Error Matrix / Total SCA 46
3.4 Fractional Statistics 47
3.5 Grain Size Retrieval Methods 53

List of Figures

2.1 Analysis Workflow 11
2.2 SNICAR Model 12
2.3 Snow Endmembers 13
2.4 Vegetation Endmembers 14
2.5 Rock, Soil, etc. Endmembers 15
2.6 Erroneous fSCA 17
2.7 Synthetic Spectral Mixture 19
2.8 Preliminary Synthetic Study 20
2.9 Final Synthetic Study 20
2.10 Optimized fSCA 22
2.11 Worflow for Single Pixel 23

3.1 Spectral Resolutions 31
3.2 Nonsnow Endmembers 36
3.3 Synthetic Spectral Mixture 39
3.4 Final Synthetic Study 40
3.5 AVIRIS flight line 42
3.6 Simulated MODSCAG 43
3.7 Simulated EnMAP 44
3.8 Histograms 02/24/16 49
3.9 Histograms 03/24/16 50
3.10 Histograms 05/18/16 51
3.11 Simulated Model Comparisons 52
3.12 Other Grain Size Retrievals 54

A.1 AVIRIS flight line like **Figure 3.5** 60
A.2 AVIRIS flight line like **Figure 3.5** 61

Chapter 1 Introduction

Seasonal snowpack is a critical water resource in many regions and mountain snow storage is also a dominant source of water for humans and ecosystems in western North America. With the highest albedo and greatest spatial extent of any other natural surface, snow-covered area (SCA) is fundamental to both hydrological, ecological, and climate models. Mountain snowpack in North America and most of Eurasia is declining as result of the warming climate and it is predicted to continue (Nolin and Daly, 2006; Stoelinga et al., 2010; Kunkel et al., 2016). When SCA diminishes as a result of seasonal changes, accurate and expedient assessment of snowmelt will improve streamflow forecasts and hydrological model simulations (Clark et al., 2006; McGuire et al., 2006; Thirel et al., 2011). The hydrological and climatological significance of this trend is unclear, but as global climate change drives down snowpack an increasing demand for improved accuracy and increased efficiency of monitoring snow's spatial extent is vital for improving model calculations.

Remote sensing is the principal and practical means of mapping snow-covered area. Spectral imaging offers quantitative information of snow in alpine regions as opposed to field measurements that would otherwise impose increased time, money, and danger. Satellite imagery and derived data products have been used to map and monitor Earth's cryosphere since the inception of the Landsat series of satellites (e.g., Hall et al., 1989; Williams et al., 1991). Early work using the Airborne Visible / Infrared Imaging Spectrometer (AVIRIS) established methods to determine both snow cover area and grain size (e.g. Painter et al. 1998). These studies were then modified to provide similar results from the coarse spatial resolution and limited spectral coverage available for more global and regional scales with the Moderate Resolution Imaging Spectroradiometer (MODIS) instrument (Dozier et al., 2008; Painter et al., 2009; Painter et al., 2012). The most accurate of these snow-covered area retrievals is the MODIS Snow-Covered Area and Grain Size (MODSCAG) retrieval algorithm

which improves upon the estimates of SCA by solving the mixed pixel problem to determine fractional snow-covered area (fSCA) with spectral mixture analysis (Painter et al., 2009; Rittger et al., 2013). Additionally, 40% of the North American seasonal snow zone is forested (Klein et al., 1998). Despite improvements in canopy adjustments (Wang et al., 2015) current MODIS canopy adjustments for fSCA indicate that snow cover is still misrepresented (Raleigh et al., 2013; Rittger et al., 2013).

The current necessities of remotely sensing fSCA are two-fold. Both a high spatial and high temporal resolution are needed for increasingly detailed hydrological, ecological, and climate inferences and modeling needs. MODIS provides fSCA, snow grain size, and other snow data products at a nominal ∼500 m spatial resolution and high 1-2 day temporal resolution. These products were integrated in a plethora of hydrologic studies and models [Parajka and Bloschl, 2008; Finger et al. 2011; Franz and Karsten, 2013; McGuire et al., 2006], but higher spatial resolution is paramount to hydrological modeling and subpixel snow spatial heterogeneity in improving runoff predictions (Luce et al., 1999; Lundquist and Dettinger, 2005; Clark et al., 2011). Snow distribution, snow cover depletion, and snowmelt for distributed hydrological modeling is often applied at 30 to 100 m resolution, (Cristea et al., 2017). However, snow cover extent and snow duration are essential to ecological studies [Choler, 2005; Venn et al., 2011; Ford et al., 2013; CaraDonna et al. 2014] on smaller spatial scales (m and tens of m) (Cristea et al., 2017). Additionally, high spatial and high temporal resolution of snow duration is needed for quantifying the effects on alpine plant habitat (Dedieu et al., 2016). High spatial resolution scanning lidar-derived snow depth data, or even IKONOS imagery are ideal products in mapping fine-scale regional snow [Painter et al., 2016; Czyzowska-Wisniewski et al., 2015], but are very challenging to collect at high temporal resolution compared to satellite imagery.

Modern airborne instrumentation provides both higher spatial and spectral resolution than current satellite imaging systems; however, products provided by the Airborne Snow Observatory (ASO) and AVIRIS are not readily available for every region or temporal resolution is too low to effectively map the transformation of snow

cover in time. Consequently, MODIS snow data products remain the best combined trade off of temporal and spatial resolution that is readily available. There have been recent efforts to refine the coarse fSCA spatial scale from ∼500 m to 3-30 m resolution through downscaling (Walters et al, 2014; Li et al., 2015; Cristea et al., 2017). Multispectral sensors like Landsat and Visible Infrared Imaging Radiometer Suite (VIIRS) have the potential to refine our spatial resolution further and release of those products is expected over the next few years (personal communication with Tom Painter). In addition, hyperspectral remote sensing is capable of resolving more snowpack properties, such as grain size, that multispectral sensing cannot. It is also unknown how valuable additional spectral resolution is to resolving forest and snow fractions in complex topography. Therefore, the advent of a high spatial and high temporal resolution satellite imaging spectrometer (IS) system would be particularly useful for snow science. Planned IS systems EnMap [Guanter, et al., 2015], slated to launch 2018, and HISUI [Matsunaga, et al., 2016], planned for inclusion on the International Space Station 2018, may provide data at new benchmark scales. Specifically, EnMap will have 30 m spatial resolution at 4 day temporal resolution (±30° off-nadir tilt). Both IS systems will also include improvements to spectral resolution (0.4-2.5 μm at ∼10 nm intervals) allowing algorithms developed for airborne instruments to be applied to satellite systems.

As part of a NASA sponsored EPSCoR Project AVIRIS data were collected along the entire Sierra Nevada mountain range extending from north of Lake Tahoe to south of Mt. Whitney during the 2015 and 2016 snow-covered season. These data span a low snow year (2015) and the melt season of a moderate snow year (2016). AVIRIS provides an equivalent aerial remote sensing product to planned IS systems on both a spectral (0.4-2.5 μm at ∼10 nm intervals) and spatial (∼15 m) scale. As an analog for future IS systems, previously collected AVIRIS data may serve the unique purpose of parameterizing the effects that future hyperspectral satellite IS systems will have on current fSCA and grain size retrieval algorithms. The goal of this work is to establish an open source snow-covered area and grain size summary product for AVIRIS that

may act as an algorithm framework for future IS systems. Additionally, the work will compare snow albedo and grain size determined using the full spectral profile from AVIRIS with the short wavelength coverage of ITRES CASI-1500 (CASI) aboard ASO, and the limited channels of MODIS.

Chapter 2 Algorithm Development

2.1 Abstract

This work builds on previous subpixel snow-covered area retrieval algorithms that take into account varying grain size. We present a model that analyzes multiple endmembers of varying snow grain size, vegetation, rock, and soil in segmented regions along the Sierra Nevada to determine snow-cover spatial extent, snow sub-pixel fraction, and approximate grain size. The root mean squared error provides a spectrum-wide assessment of the mixture model's goodness-of-fit. The development of the model is based on Airborne Visible/Infrared Imaging Spectrometer (AVIRIS) data that were collected along the entire Sierra Nevada mountain range during the 2015 and 2016 snow-covered season. The AVIRIS dataset used in this experiment consists of 224 contiguous spectral channels with wavelengths ranging 400-2500 nanometers at a 15-meter spatial pixel size. However, the model allows input parameters to vary for different endmembers, spectral or spatial resolutions, and other algorithm thresholds. Future plans to make the model open-source may allow additional optimization and applications to other IS systems.

2.2 Introduction

The H_2O molecule has a very characteristic spectral shapes in both liquid and solid forms (e.g. Green et al., 2006; Dozier et al., 2009). Aerial and satellite remote sensing effectively detect snow cover due to snow's characteristic spectral shape which is easily distinguishable from vegetation, soil, rock, water, etc. (Dozier, 1989, see also **Figures 2.2** and **2.4**). The normalized difference snow index (NDSI) differentiates snow from other land features (Dozier, 1989). NDSI is calculated by normalizing the difference of the reflectance in the visible spectrum (RVIS) from the reflectance in the near infrared (RNIR). When NDSI is greater than 0.4 then the pixel is denoted as a snow-covered

pixel (Dozier, 1989).

$$NDSI = \frac{R_{VIS} - R_{NIR}}{R_{VIS} + R_{NIR}}$$

However, this unsupervised classification scheme is binary- a pixel is either snow or not snow. Traditional supervised and unsupervised classifications of snow cover are problematic for mixed pixel areas composed of snow, rock, vegetation, water, ice, etc. which makes it difficult to assess what percentage of snow actually covers the pixel. A fractional snow-covered area (fSCA) product was developed for MODIS based on an empirical relationship between fSCA and the NDSI (Salomonson and Appel, 2004; Salomonson and Appel, 2006). The MODIS derived data products, MOD10AI (Terra) and MYD10A1 (Aqua) are fractional models that utilize bands centered in the visible and NIR:

MOD10A1:

$$f_{SCA} = -0.01 + 1.45(NDSI),\ where\ NDSI = \frac{R_4 - R_6}{R_4 + R_6}$$

Where R_4 is centered on MODIS band 4 (0.555 μm) and R_6 on MODIS band 6 (1.640 μm).

MYD10A1:

$$f_{SCA} = -0.64 + 1.91(NDSI),\ where\ NDSI = \frac{R_4 - R_7}{R_4 + R_7}$$

Where R_4 is centered on MODIS band 4 (0.55 μm) and R_6 on MODIS band 6 (2.130 μm).

However, these fSCA products are not significantly better than the binary method and are also substantially worse than spectral mixture analysis fSCA products when

validated with fSCA from the Landsat Enhanced Thematic Mapper (ETM+) (Rittger et al., 2013).

2.2.1 Linear Spectral Mixture Analysis in Snow Science

Linear spectral mixture analysis assumes that each pixel is a collection of constituent spectra, or chosen endmembers (i.e., snow, vegetation, rock, etc.) and 'unmixes' their corresponding fractions that compose each pixel. The spectral mixture analysis was first used to map snow-covered area by Nolin et al. (1993) and is based on the following equation:

$$R_c = \sum_{i=1}^{N} F_i R_{i,c} + E_c \tag{2.1}$$

Where R_c is the apparent surface reflectance in band c, F_i is the fraction of endmember i, R_{ic} is the reflectance of endmember i in band c, N is the number of spectral endmembers, and E_c is the residual error in band c for the fit of the N endmembers (Gillespie et al., 1990).

Large spectral libraries determine what endmembers to use, and can depend on the region (Painter et al., 2003). Additionally, multiple snow endmembers are necessary to accurately determine subpixel snow-covered area (Painter et al., 1998). Past work has been successful in mapping fractional snow-covered area, evolution of snow grain size, fraction of liquid water in the surface layer, and contaminants that decrease the albedo, such as dust, soot and algae (e.g. Nolin et al. 1993; Painter et al. 1998; Nolin and Dozier 2000; Painter et al. 2003; Green et al. 2006; Dozier et al. 2009; Nolin 2010).

In the MODIS snow product suite the most accurate snow-covered area data is the MODSCAG algorithm which improves upon the estimates of SCA by solving the mixed pixel problem to determine fSCA with spectral mixture analysis (Painter et al., 2009; Rittger et al., 2013). MODSCAG uses a snow endmember library generated with a radiative transfer model to produce hemispherical-directional reflectance for

monodispersions of spheres at varying solar zenith angles (Painter et al., 2009). The algorithm solves equation (2.1) for the error, which provides us with the residuals, and to measure the spectrum-wide quality of fit we average the root mean squared error (RMSE):

$$E_c = R_c - \sum_{i=1}^{N} F_i R_{i,c} \tag{2.2}$$

$$RMSE = [M^{-1} \sum_{c=1}^{M} E_c^2]^{1/2} \tag{2.3}$$

M is the number of bands in the spectral mixture analysis. Dennison et al. (2003) have shown that RMSE is best for determining overall goodness of fit in spectral unmixing. The fraction endmembers are determined and MODSCAG includes the following constraints: (a) a model is considered valid if fractions are in the range [-0.01,1.01] (b) overall RMSE $< 2.5\%$, and (c) no three spectrally consecutive residuals exceed 2.5% (Painter et al., 2009). Pixels outside of these constraints are modeled more loosely with the following constraints: (a) [-1.01,2.01] (b) overall RMSE $< 5\%$, and (c) no three spectrally consecutive residual exceed 5%. The estimation of subpixel snow-covered area is derived from the shade-normalized snow fraction.

$$f_s = \frac{F_s}{\sum_{p \in s,v,r} F_p} = \frac{F_s}{1 - F_{shade}} \tag{2.4}$$

F_s is the snow spectral fraction, F_p are the physical spectral fractions snow, vegetation, rock, etc. By normalizing the additive complement of the shade fraction topographic effects of shadowing and illumination are accounted for (Adams et al., 1993; Painter, 1998; Painter et al., 2003).

Therefore, each pixel is subjected to an n-choose-k problem of varying snow grain size (snow endmembers), vegetation, rock/soil, and photometric shade. The fractional combinations and associated RMSE of these mixtures are then compared. For

MODSCAG, models with three or more endmembers constitute an accepted mixture analysis. MODSCAG attributes the pixel with the fewest endmembers and lowest RMSE (within the constraint) to the fractional combinations provided. For example, a single pixel will first be tested by the collection of three-endmember models (this could be a snow endmember, vegetation, rock, soil etc. plus a photometric shade endmember). This model may likely not be within the RMSE threshold or other constraints, and thus the pixel is tested by the collection of four-endmember models, and so on until the constraints are met. The collection of endmembers and their associated fractions with the lowest overall RMSE are then chosen to represent that pixel.

2.2.2 Preliminary Algorithm

Initial attempts at determining fSCA and subsequent grain size were based on spectral mixture analysis following equation (2.1). However, unlike MODSCAG that uses a large array of varying physical endmembers, our endmember selection was crudely chosen in-scene. The entire algorithm process can be summarized in three steps. Step (1), Dimension reduction of initial hyperspectral flight line into original flight line width ∼850-1000 pixels by a length of 1000 pixels. This step was necessary to reduce the ∼30 GB flight lines to smaller sizes that are more rapidly processed. Step (2), Automated endmember determination. If the pixel NDSI value is greater than 0.4 and its original reflectance at ∼695 nm is greater than 0.11 the pixel is defined as clear snow. This is common practice for binary snow metrics (Dozier, 1989). Two vegetation and two rock endmembers were determined by an algorithm based on NDVI and reflectance values (at 860-1101 and 404-647 nm). In addition, multiple snow endmembers of varying grain sizes based on a band feature area at ∼1030 nm (Nolin 2000) were chosen. For all endmembers, since they were chosen in the scene, atmospheric correction artifacts were masked. Step (3), Inversion. Assuming a flat spectrum for our shade endmember, a linear spectral mixture analysis determines the RMSE and subpixel percent at each pixel for each snow endmember. The grain size

with the lowest RMSE and corresponding subpixel percent is chosen in final RMSE and subpixel percentage plots. Steps 1-3 are then repeated for each subsequent subset of the total flight line.

This process was a good platform for getting familiar with the spectral mixture analysis method, but was inadequate to provide consistent characterization of snow across flightlines, years, and seasons. The algorithm did not include pure endmembers or an RMSE threshold, and limiting the model to three endmembers did not allow choosing the most parsimonious solution.

2.3 Model Description

Our model and algorithm is based on MEMSCAG (multiple endmember snow-covered area and grain size) that was derived from MESMA (multiple endmember spectral mixture analysis) (Painter et al., 2003; Robert et al., 1998). Our model simultaneously derives fSCA and snow grain size from a constrained linear spectral mixture analysis. We provide detail to the input parameters, model specifications, and improvements to optimization that has evolved and led to our current model. **Figure 2.1** describes the workflow for our analysis. Unlike MEMSCAG, which is coupled with its own radiative transfer model and in situ measurements, we have produced our own endmember library.

2.3.1 Development of Endmembers

As discussed previously, spectral mixture analysis assumes that each pixel's reflectance is a linear combination of a set of selected endmembers. It is very important that each endmember (i.e., snow, vegetation, rock, etc.) is as spectrally pure as possible (Painter et al., 2003). Previous methods either masked out snow cover fractions that were less than 90% due to anomalously high grain size values that were the result of mixtures of snow, vegetation, and rock or looked at small spatial areas and assumed only or one or two additional vegetation and rock endmembers (Painter et al. 1998;

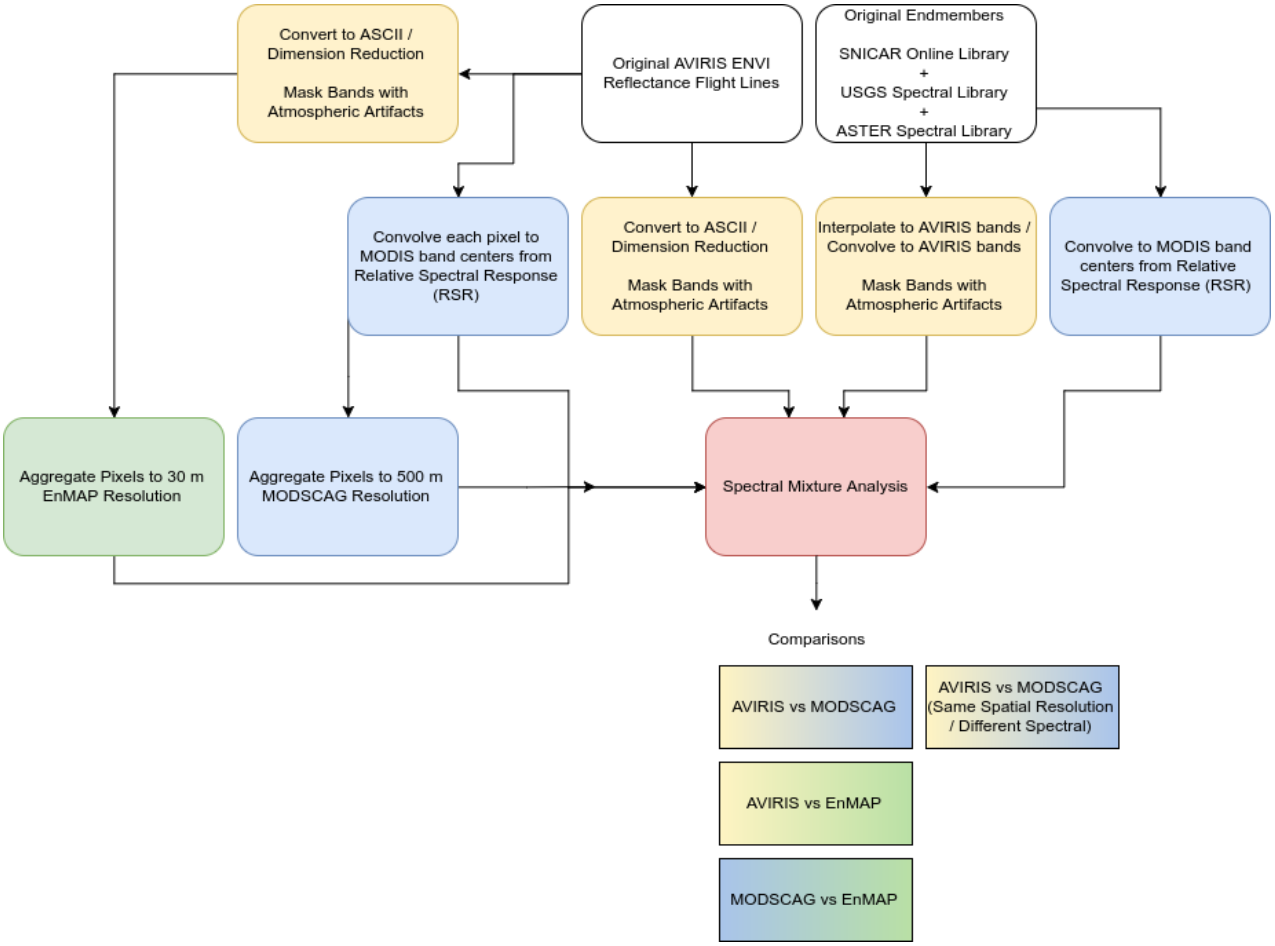

Figure 2.1: Workflow describing the necessary procedures that leads to different IS comparisons. It should be noted, while not included for our comparison, that this model can easily include other multispectral satellites such as Landsat or Sentinel-2.

Nolin and Dozier, 2000). MEMSCAG incorporated 60 spectral endmembers for vegetation, rock, soil, and lake ice in the Sierra Nevada taken with an Analytical Spectral Devices FieldSpec FR field spectroradiometer for use in an AVIRIS snow-covered area retrieval algorithm (Painter et al., 2003).

We interpolate snow endmembers from the Snow, Ice, and Aerosol Radiation (SNICAR) model available online at the University of Michigan **Figure 2.2** (Flanner et al. 2007; 2009).

Among many other parameters, the SNICAR model allows for snow grain sizes ranging from 30-1500 microns. Since MODSCAG makes use of a snow endmember

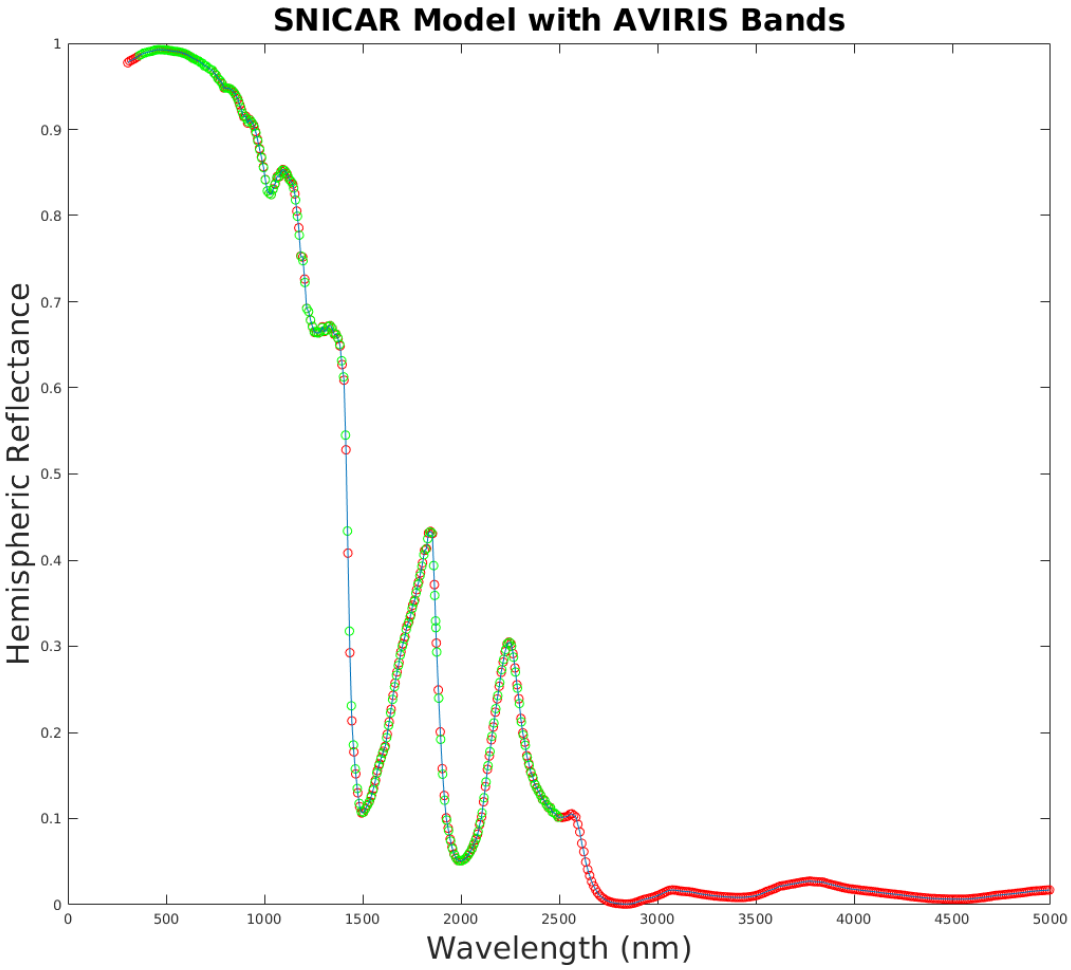

Figure 2.2: SNICAR model ranging from 305-5000 nm at 10 nm intervals for 100 μm snow grain size (red dots) with the 224 AVIRIS bands weighted to the SNICAR model albedo values (green dots).

library from 10-1100 microns at 10 micrometer intervals we too develop a snow endmember library of similar caliber for each of our AVIRIS scenes. The AVIRIS flights provide the solar elevation angle. From solar elevation angle we input a solar zenith angle as a parameter into the SNICAR model and produce varying snow grain sizes from 30 to 1100 micrometers at 10 micrometer intervals. **Figure 2.3** is an example of a 108 snow endmember library interpolated to AVIRIS bands.

Vegetation, rock, soil, etc. endmembers were measured in situ in the region of

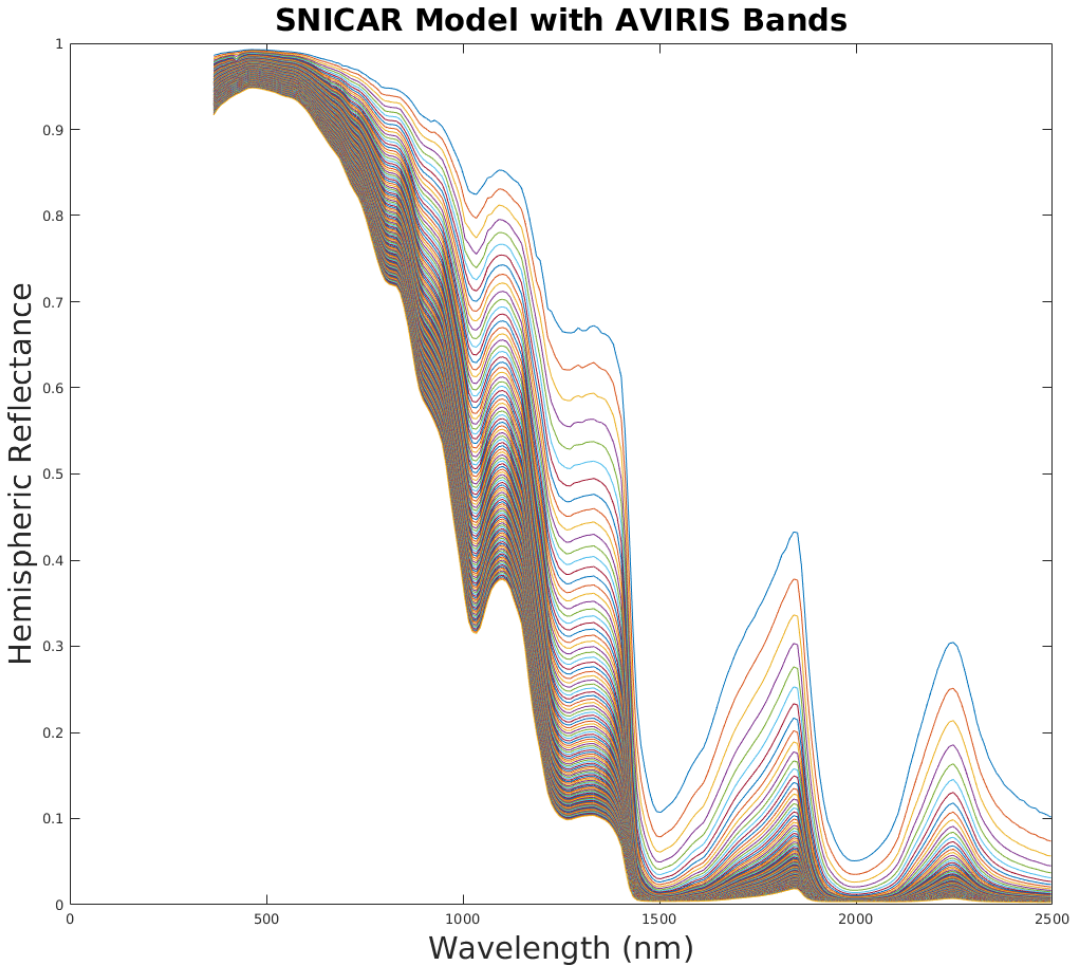

Figure 2.3: An example of our snow endmember library for a single flight line. The SNICAR model of 108 snow endmembers varying from 30-1100 micrometers interpolated to AVIRIS channels.

Sage Hen. However, we opted to not use these measurements as the local vegetation species and mineralogy changes throughout the entire Sierra Nevada region. We therefore decided to produce a generalized endmember library for typical vegetation and minerals/soils found in the Sierra Nevada. We interpolated and convolved vegetation, rock, soil, etc. endmembers from the USGS Spectral Library Version 7 [Kokaly et al., 2017] and from the ASTER Spectral Library Version 2.0 [Baldridge et al., 2009] to AVIRIS channels **Figure 2.4** and **Figure 2.5**. Spectra that were sampled

at a spectral resolution finer than AVIRIS were convolved to the AVIRIS channels with a Gaussian bandpass filter (Painter et al., 2003). We masked spectral channels where there were high atmospheric correction artifacts present in our data (around 1400 and 1900 nm). This model does not attempt to identify vegetation species or rock/soil mineralogy, so attention to specific bidirectional reflectance is not necessary and assumed nadir (Painter et al., 2003).

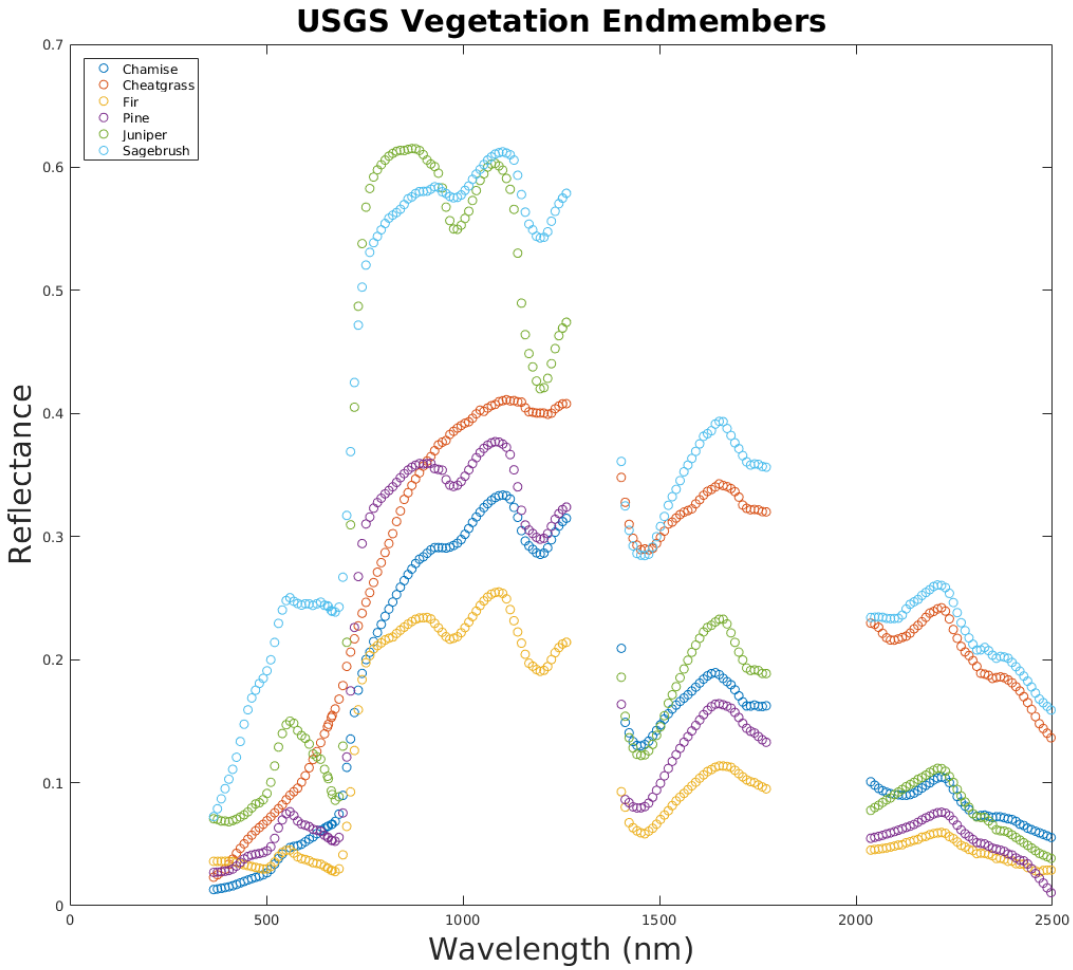

Figure 2.4: Six vegetation endmembers common to the Sierra Nevada taken from the USGS Spectral Library Version 7. Original names provided in index.

Of the endmembers chosen, preliminary spectral mixture analysis of the Sage Hen study site indicated that over 90% of mixed pixels were attributed to vegetation

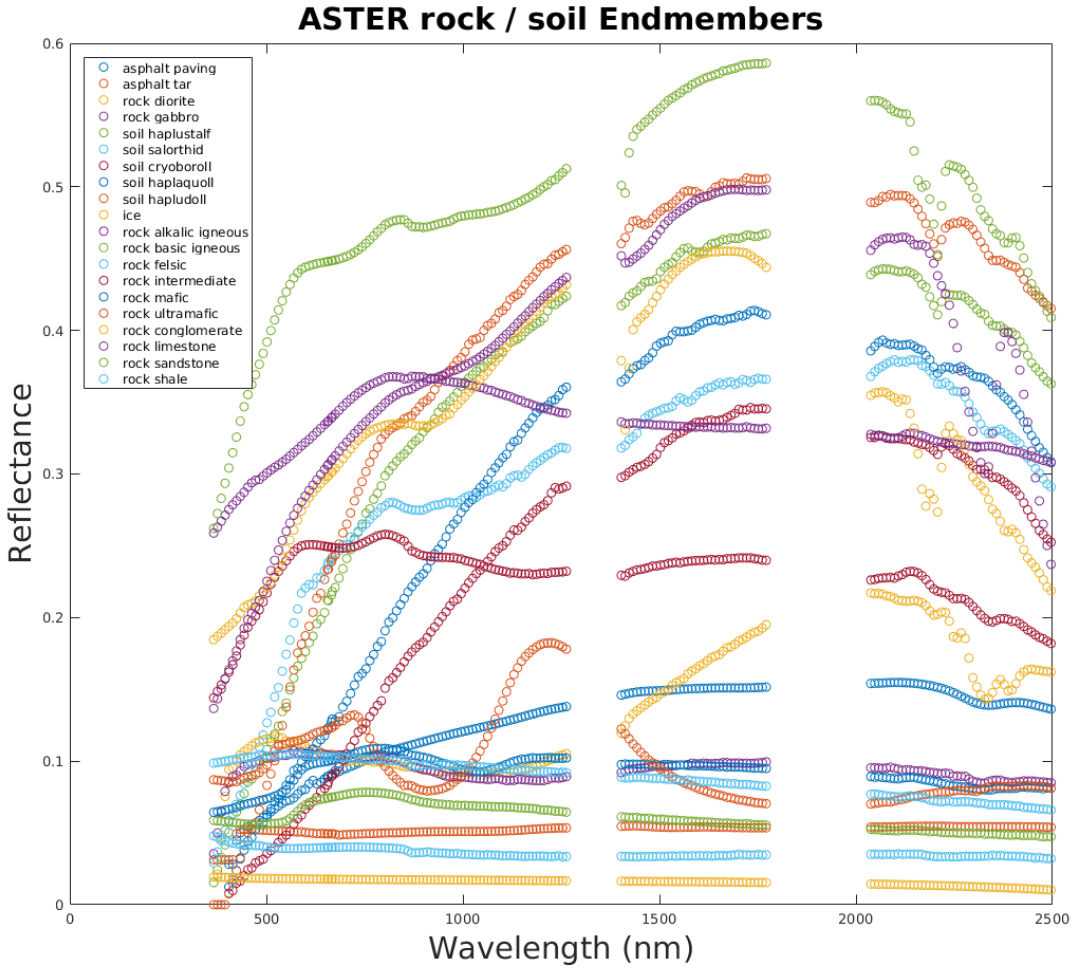

Figure 2.5: Rock, soil, ice, and asphalt common to the Sierra Nevada taken from the ASTER Spectral Library Version 2.0. Original names provided in the index.

endmembers, and 100% of mixed pixels were attributed to only 10 endmembers (of a 26 total) outside of our snow endmembers. Therefore, to improve on computation times, we reduced the non-snow library to these 10 endmembers (**Figure 3.2**). It will be necessary to to do full library inversions at spatially random intervals throughout an entire flight line in the future to decide how valid this reduction is.

2.3.2 Development of Spectral Mixture Analysis

The brunt of the computational effort that goes towards solving equation (2.1) is the Matlab R2016a function available in the Optimization toolbox called lsqlin (R2016a, The MathWorks, 2016). The function allows us to optimally solve the constrained linear least-squares problem. Earlier versions of our model replicated the constraints of previous work to varying degrees (Nolin and Dozier 2000; Painter et al., 2003; Painter et al., 2009). We include the constraints that since we are only interested in fSCA and grain size to ignore pixels that have an NDSI < 0.0, the spectral fractions must sum-to-unity, spectral fractions are in the range [-0.01, 1.01], overall RMSE $< 5\%$ (Compared to MEMSCAG and MODSCAG which is 2.5%), and unlike MEMSCAG or MODSCAG we ignore spectrally consecutive residuals exceeding our RMSE threshold of 5%. The NDSI threshold improves computation times instead of looking at each pixel, and since spectral mixture analysis is only accurate down to 15% snow cover the NDSI threshold includes this region in all endmember combination cases (Rittger et al., 2013). The 5% RMSE threshold, while computationally less expensive than 2.5% resulted in erroneous fSCA and grain size calculations as discussed later.

Since spectral mixture analysis assumes that the reflectance spectrum of a single pixel is a combination of varying endmembers, it is mathematically possible to have that spectrum be accurately represented by different n-endmember combinations. However, the solutions with a larger number of endmembers are mathematically trivial solutions and also likely unrealistic. It is easier to model a vector with an increasing number of basis vectors that are not degenerate (Painter et al., 2009). Thus, the chosen fSCA and grain size must first pass the constraints of the spectral mixture analysis and also have the fewest endmembers- i.e. the parsimonious solution. To save on computation times we implement the parsimonious solution by wrapping the spectral mixture analysis with an RMSE threshold check. While this reduces computation times instead of checking a pixel for varying n-endmember combinations, it also resulted in erroneous fSCA and grain size calculations.

The results of the early implementations and how errors were manifested is shown

in **Figure 2.6**. Here the approximate true color image compared to the shade normalized subpixel snow fraction (derived from equation 2.4). The true color image depicts the snow cover as significantly more varied than pure snow. However, our early model results indicate that there is nearly 100% snow cover (maroon pixels) over the vast majority of the scene. In order to understand why our model was erroneously overestimating fSCA we performed a sensitivity analysis.

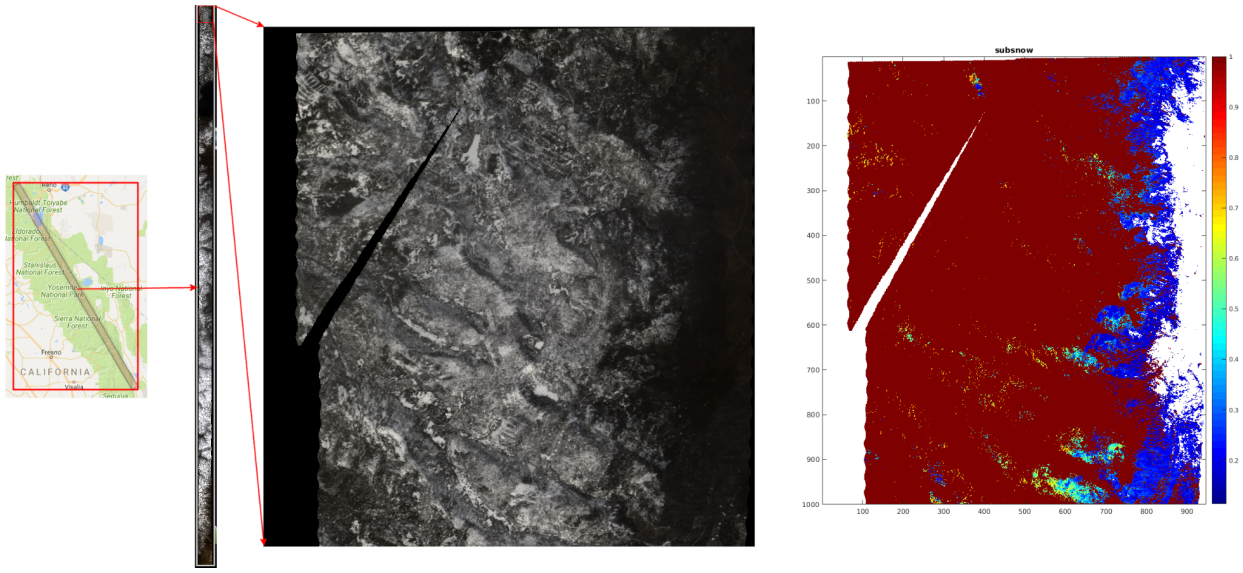

Figure 2.6: Depicts the erroneous fSCA from earlier algorithm results. The red pixels on the right represent 100% snow cover, but when we view the true color on the left snow cover is much more variable. The sensitivity analysis would provide insight to understand why this was happening.

2.4 Sensitivity Analysis

We performed a synthetic study to understand the sensitivity of our model's ability to determine fSCA and grain size for varying snow grain sizes and different endmembers [Painter et al., 2003]. The simulated pixel is a linear combination of a single snow grain size endmember and another endmember (vegetation) varying from 0 to 100%, incremented by 10% mixtures **Figure 2.7**. In our earlier model, which uses a 5% RMSE threshold, modelled fSCA is accurate only to ∼70% true snow cover area and overestimates snow cover by ∼30%, improving with larger snow grain sizes as

shown in **Figure 2.8**. Ideally, our shade normalized fSCA (circles on graph) should follow the 1:1 line, but consistently overestimates fSCA above ∼70% snow cover. The shade not-normalized fSCA (asterisks in **Figure 2.8**) is consistently closer to the true fSCA, but for entirely wrong reasons. That is is to say the shade not-normalized fSCA is closer to the true value, but only because the model chooses the wrong grain size for these snow and shade only combinations. Similarly, discrepancies in modelled grain size parallel discrepancies in fSCA. In all erroneous instances, grain size is underestimated. We find that these results are due to the model choosing the most parsimonious solution first. Since shade is an endmember always present, our model will determine a pixel is purely snow (combined with a shade endmember-equation (2.4)) if that combination is below the 5% RMSE threshold, as opposed to a combination of snow and another endmember first. Therefore the model will prefer a single snow endmember that is of a lower grain size combined with shade over the correct snow endmember combined with vegetation or comparatively whatever true endmember is present. The quick solution was to simply set a lower RMSE threshold, but this increased computation times drastically. We have adjusted the algorithm to minimize these errors and maintain relatively efficient computation times.

2.5 Final Improvements

To increase the accuracy for large snow covered pixels while maintaining realistic computation times two adjustments to the workflow were implemented. The first adjustment was to set an NDVI threshold check before the parsimonious solution spectral mixture analysis. A pixel that has an NDVI greater than 0.2 is immediately assumed to be more than a combination of snow and shade and the computation thereby avoids the first iteration of the of 2-endmember solutions (i.e. snow and shade). Instead the algorithm will proceed with combinations of 3-endmember solutions or more. We do not limit the solution matrix to only vegetation endmembers, but in the future this might be an improvement to computation times to do so. The second adjustment was to set a lower RMSE threshold for 2-endmember solutions as opposed to

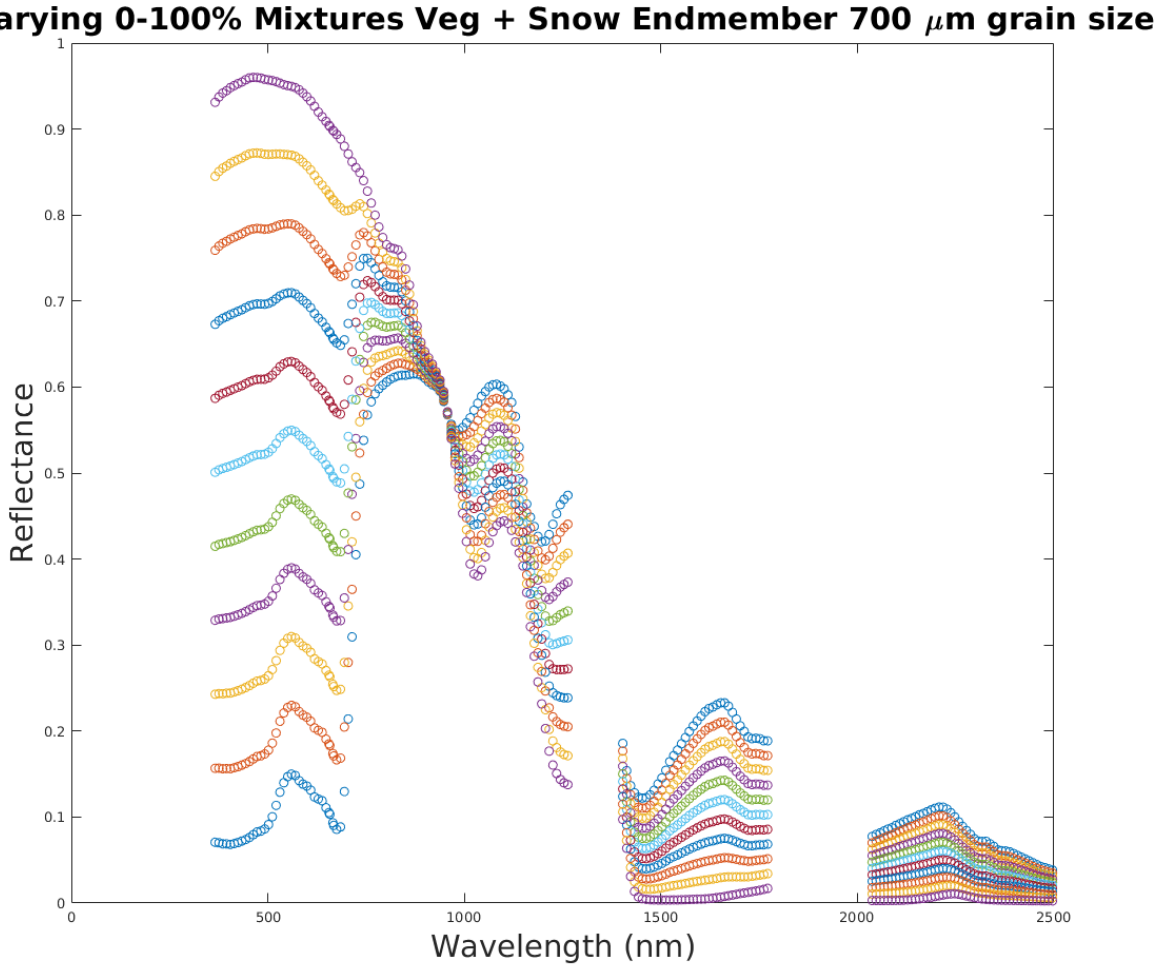

Figure 2.7: Example of synthetic spectral mixtures from the sensitivity study. Mixtures vary from 100% snow 0% vegetation to 0% snow 100% vegetation in 10% increments. Snow endmember shown is 700 μm grain size and vegetation endmember shown is juniper.

3-endmember solutions or more. Since the main source of error in overestimation of fSCA and consequent underestimation of grain size was due to the algorithm choosing a lower grain size combined with shade over the true grain size and true endmember combination, we set a lower 2% RMSE threshold for all 2-endmember solutions (i.e. snow and shade will only be a chosen combination for a pixel if the RMSE is $< 2\%$). This increases computation times, but significantly improves accuracy. **Figure 2.9** depicts the improvements in the refined model with a sensitivity analysis and **Figure**

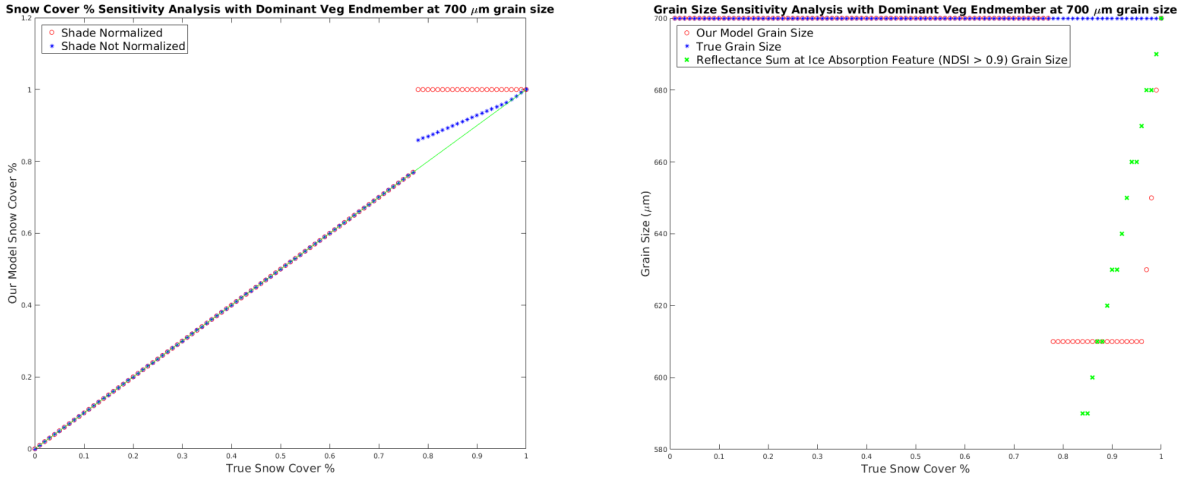

Figure 2.8: Synthetic sensitivity modeling results for 700 μm grain size at 5% RMSE threshold. The left graph shows that the shade-normalized unmixing begins to over predict snow at 70% true snow cover. The right graph shows that the modeled grain size underestimates true grain size and parallels these errors.

2.10 shows the examples of a true color and subsequent fSCA calculations. In implementing these adjustments, fSCA is only overestimated at ∼85-99% true snow cover area, but only overestimating by <15%. Similarly, grain size is only underestimated at the highest snow cover fractions.

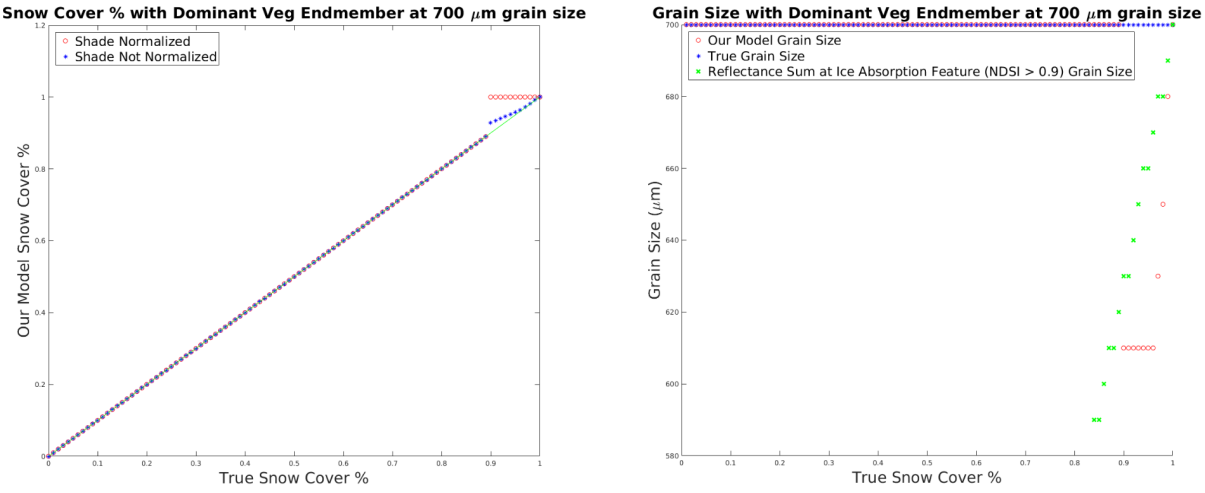

Figure 2.9: Synthetic sensitivity modeling results for 700 μm grain size for optimized model.

Finally, a new method to improve computation times was implemented that divides the spectral mixture analysis into two runs. Since the number of snow endmembers is 108 (30-1100 at 10 μm intervals) each n-choose-k problem is on the order of 108 endmembers plus 10 non-snow endmembers. Instead, we divide the snow endmembers into a preliminary grouping and then a final grouping based on the results of the first spectral mixture analysis run. The first spectral mixture analysis will look at a smaller subset of snow endmembers (100-1100 at 100 μm intervals) for a total of 11 snow and 10 non-snow endmembers. From this first run, the selection is narrowed further in the second run to snow endmembers that vary from the 10 μm intervals before and after the chosen endmember. For example, a pixel will first look at the 11 snow and 10 non-snow endmembers, and might choose an n-endmember combination that uses the 200 μm grain size snow endmember. Then, on the second run, the snow endmembers that are the new input parameters to the spectral mixture analysis range from 110-290 μm at 10 μm intervals. This method improves computation times drastically and appears to not have any limiting effects on accuracy. These combined adjustments to the spectral mixture analysis algorithm is what our current and best model incorporates. The details of the workflow for the single 'Spectral Mixture Analysis' box in **Figure 2.1** is summarized in **Figure 2.11**. We plan to share the project on the Matlab File Exchange to allow for future optimization and community improvements using an open license.

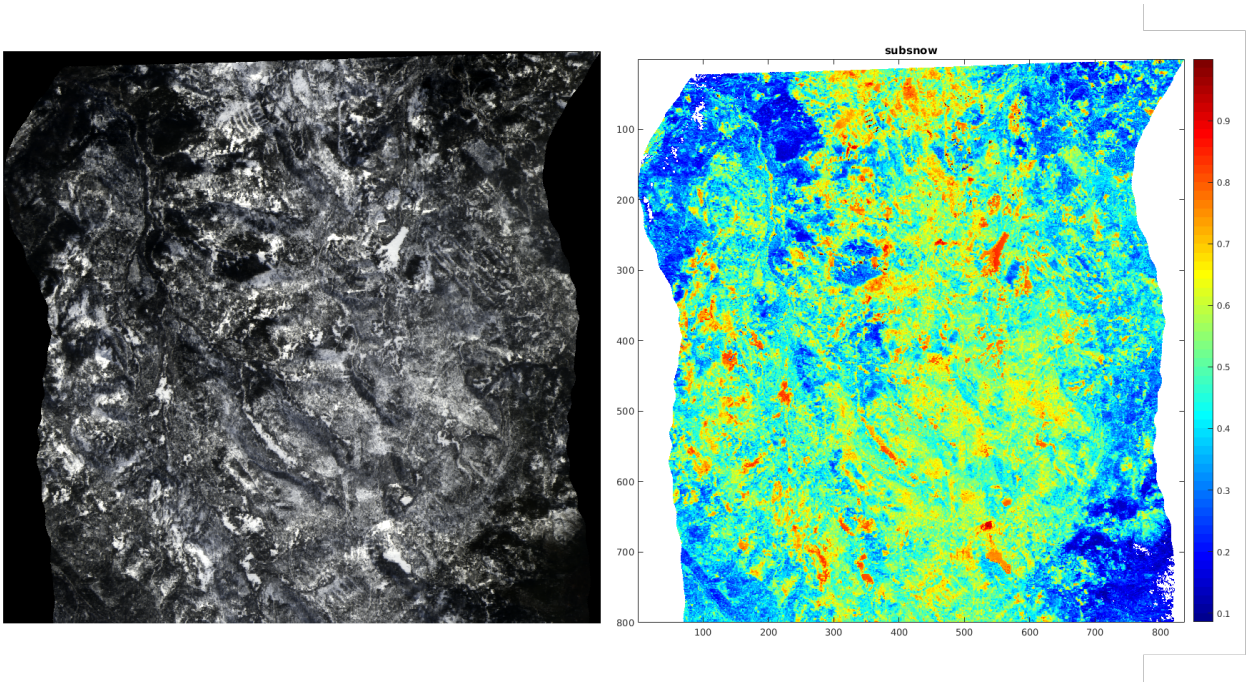

Figure 2.10: Depicts an approximate true color subsection of one of our flight lines on the left, and on the right the fSCA from our optimized algorithm.

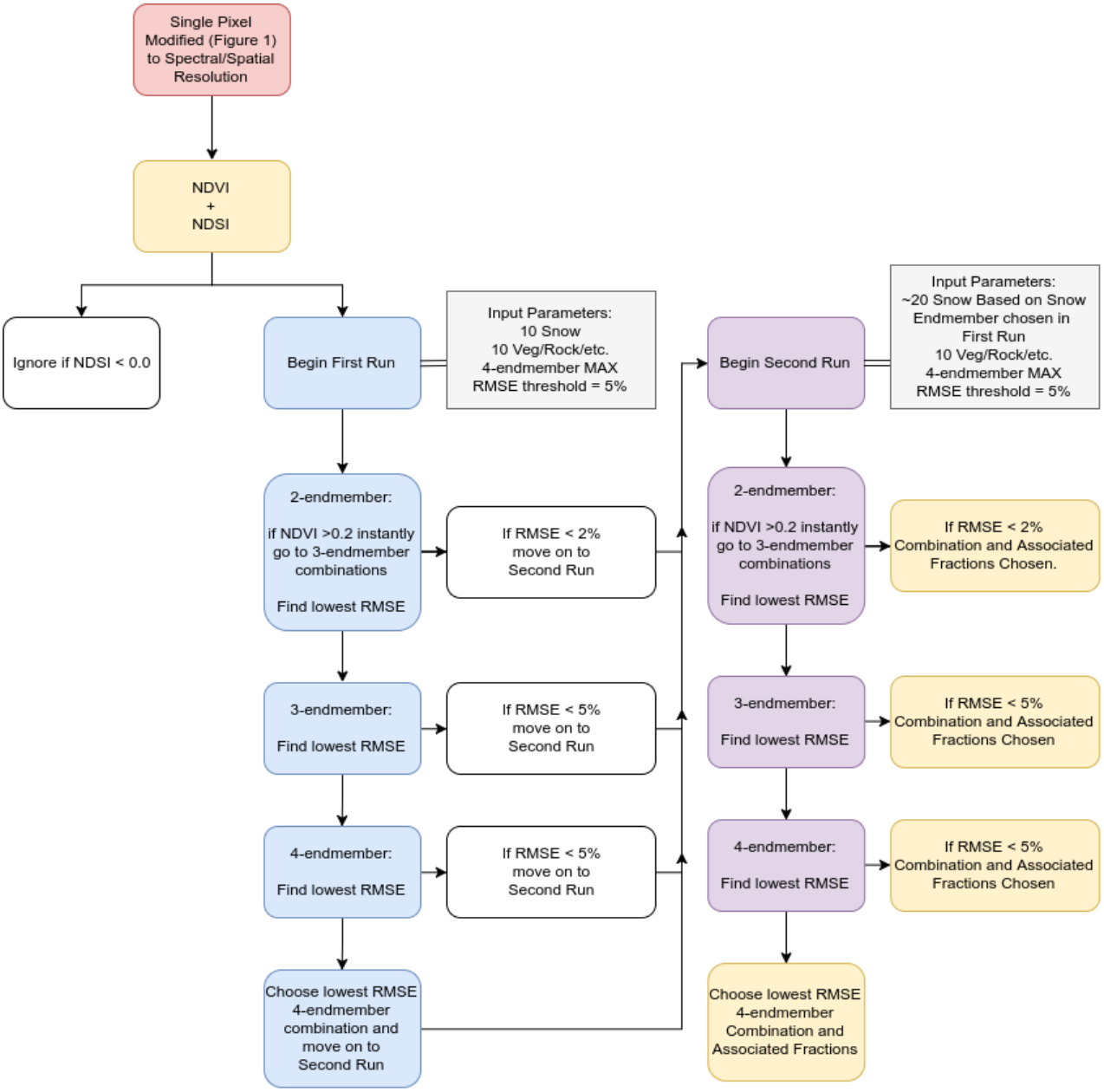

Figure 2.11: Workflow of the finalized spectral mixture analysis section from **Figure 2.1**. Orange boxes are recorded in the final output for each pixel.

Chapter 3 Manuscript for submission to Remote Sensing of Environment; Title: Next Generation Snow Cover Mapping: How Future Hyperspectral Satellite Spectrometer Systems Can Improve Subpixel Snow-covered Area and Grain Size

3.1 Abstract

Mountain snow storage is the dominant source of water for humans and ecosystems in semiarid western North America. Consequently, the spatial distribution of snow-covered area is fundamental to both hydrological, ecological, and climate models. Airborne Visible/Infrared Imaging Spectrometer (AVIRIS) data were collected along the entire Sierra Nevada mountain range extending from north of Lake Tahoe to south of Mt. Whitney during the 2015 and 2016 snow-covered season. Data from the Sierras were acquired on four days: 2/24/15 during a very low snow year, 3/24/16 near maximum snow accumulation, and 5/12/16 and 5/18/16 during snow ablation and snow loss. This study focuses on the Sagehen Creek Field Station (39°25'54.7'' N 120°14'26.67'' W) and the surrounding watershed for an approximate 20 km x 1.5 km area. Building on previous retrieval of subpixel snow-covered area algorithms that take into account varying grain size we present a model that analyzes multiple endmembers of varying snow grain size, vegetation, rock, and soil to determine snow-cover spatial extent, snow sub-pixel fraction, and approximate grain size. In addition, varying simulated models of the data compare and contrast the retrieval of current snow products such as MODIS Snow-Covered Area and Grain Size (MODSCAG) and the ITRES CASI-1500 (CASI) aboard the Airborne Snow Observatory (ASO), and future hyperspectral satellite spectrometer systems. Specifically, does lower spatial resolution (MODIS), fewer spectral channels (MODIS), and limited spectral resolution (CASI) affect snow-cover area and grain size approximations? The implications of our findings will help refine snow mapping products for planned hyperspectral satellite spectrometer systems such as EnMAP (slated to launch in 2019), HISUI (planned for

inclusion on the International Space Station in 2018), and HyspIRI (currently under consideration).

Keywords: Snow, Imaging Spectroscopy, AVIRIS, Spectral mixture analysis

3.2 Introduction

Seasonal snowpack is a critical water resource in many regions with mountain snow storage as the dominant source for humans and ecosystems in western North America. With the highest albedo and greatest spatial extent of any other natural surface, snow-covered area (SCA) is fundamental to both hydrological, ecological, and climate models. Mountain snowpack in North America and most of Eurasia is declining as result of the warming climate and it is predicted to continue (Nolin and Daly, 2006; Stoelinga et al., 2010; Kunkel et al., 2016). When SCA diminishes as a result of seasonal changes, accurate and expedient assessment of snowmelt will improve streamflow forecasts and hydrological model simulations (Clark et al., 2006; McGuire et al., 2006; Thirel et al., 2011). The hydrological and climatological significance of decreasing SCA is unclear, but as global climate change drives down snowpack an increasing demand for improved accuracy and increased efficiency of monitoring snow's spatial extent is vital for improving model calculations.

Early work using the Airborne Visible / Infrared Imaging Spectrometer (AVIRIS) established methods to determine both snow cover area and grain size (e.g. Painter et al., 1998; Painter et al., 2003). These studies were then modified to provide similar results from the coarse spatial resolution and limited spectral coverage available for more global and regional scales with the Moderate Resolution Imaging Spectroradiometer (MODIS) instrument (Dozier et al., 2008; Painter et al., 2009; Painter et al., 2012). Despite the need for higher fidelity snow information (e.g. fractional snow-covered area (fSCA) and albedo), we are still challenged by unmixing pixels that are a combination of several land use classes. The most accurate of these snow-covered area retrievals is the MODIS Snow-Covered Area and Grain Size (MODSCAG) retrieval algorithm which improves upon the estimates of SCA by solving the mixed

pixel problem to determine fSCA with spectral mixture analysis (Painter et al., 2009; Rittger et al., 2013).

Modern airborne instrumentation provides both higher spatial and spectral resolution than current satellite imaging systems; however, products provided by ASO and AVIRIS are not readily available for every region or temporal resolution is too low to effectively map the transformation of snow cover in time. Consequently, MODSCAG remains the best combined trade off of temporal and spatial resolution that is readily available. There have been recent efforts to refine the coarse fSCA spatial scale from ∼500 m to 3-30 m resolution through downscaling (Walters et al, 2014; Li et al., 2015; Cristea et al., 2017). Multispectral sensors like Landsat and Visible Infrared Imaging Radiometer Suite (VIIRS) have the potential to refine our spatial resolution further and release of those products is expected over the next few years (Justice et al., 2013). In addition, hyperspectral remote sensing is capable of resolving additional snowpack properties, such as grain size, that multispectral sensing cannot. It is also unknown how valuable additional spectral resolution is to separating forest and snow fractions in complex topography. Therefore, the advent of a high spatial and high temporal resolution satellite imaging spectrometer (IS) system would be particularly useful for snow science. Planned IS systems EnMap [Guanter, et al., 2015], slated to launch 2018, and HISUI [Matsunaga, et al., 2016], planned for inclusion on the International Space Station 2018, may provide data at new benchmark scales. Specifically, EnMap will have 30 m spatial resolution at 4 day temporal resolution (±30° off-nadir tilt). Both IS systems will also include improvements to spectral resolution ((0.4-2.5 μm at ∼10 nm intervals) allowing algorithms developed for airborne instruments to be applied to satellite systems. As an analog for future IS systems, previously collected AVIRIS data serve to parameterize the effects that future hyperspectral satellite IS systems will have on current fSCA and grain size retrieval algorithms.

3.3 Background

3.3.1 Snow Covered Area

Of the MODIS snow products, the most accurate snow-covered area product is MODSCAG which simultaneously determines fSCA and snow grain size with linear spectral mixture analysis (Painter et al., 2009; Rittger et al., 2013). Linear spectral mixture analysis assumes that each pixel is a collection of constituent spectra, or chosen endmembers (i.e., snow, vegetation, rock, etc.) and 'unmixes' their corresponding fractions that comprise each pixel. The spectral mixture analysis was first used to map snow-covered area by Nolin et al. (1993) and Painter et al. (1998) and is based on the following equation:

$$R_c = \sum_{i=1}^{N} F_i R_{i,c} + E_c \tag{3.1}$$

Where R_c is the apparent surface reflectance in band c, F_i is the fraction of endmember i, R_{ic} is the reflectance of endmember i in band c, N is the number of spectral endmembers, and E_c is the residual error in band c for the fit of the N endmembers (Gillespie et al., 1990).

Large spectral libraries determine what endmembers to use, and can depend on the region (Painter et al. 2003). Past work has been successful in mapping fractional snow cover area, evolution of snow grain size, fraction of liquid water in the surface layer, and contaminants that decrease the albedo, such as dust, soot and algae (e.g. Nolin et al. 1993; Painter et al. 1998; Nolin and Dozier 2000; Painter et al. 2003; Green et al. 2006; Dozier et al. 2009; Nolin 2010).

3.3.2 Snow Grain Size

Snow grain size is what determines the spectral albedo in the near-infrared wavelengths (Wiscombe & Warren, 1980). When impurities in the snowpack are not present snow surface grain size is an important indicator of snow metamorphism and

also provides a foundation from which to determine radiative forcing (Painter et al., 2016). The wavelength range of 1000-1300 nm is where snow's spectral reflectance is most sensitive to grain size, and therefore instruments with high spectral resolution in this range can provide the most robust measures of grain size (Painter et al., 2003). Nolin and Dozier (1993; 2000), developed and then improved upon a method for remotely sensing snow grain size by integrating across an entire 1030 nm absorption feature and then scaling by its continuum. Their model has a grain diameter uncertainty of $\pm$20-50 μm across the grain radius range of 50-900 μm. Additionally, these early methods were constrained to pixels that were entirely snow-covered (Nolin & Dozier, 1993; Nolin & Dozier, 2000; Green et al., 2002). Despite this sensitivity to pure snow pixels, similar approaches to this absorption feature method are still used in determining snow grain size (Painter et al., 2013; Painter et al., 2016). Because examples of this method are under the assumption that a pixel is pure snow they assume that a pixel is clear snow if the NDSI > 0.9 (Painter et al., 2013), or since the spatial resolution is high (ASO $\sim$3 m) then a pixel is classified as snow or not snow and not a mixed pixel (Painter et al., 2016).

Another method for determining snow grain size is entirely based on the spectral mixture analysis. The spectral mixture analysis assumes multiple combinations of two or more endmembers of the spectral library, while maintaining only one snow endmember (Painter et al., 1998; Painter et al., 2003; Painter et al., 2009). Therefore, since the snow endmember library is based entirely on snow at varying grain sizes the mixture of a certain pixel with the lowest RMSE, and additional constraints, will be attributed to a specific snow grain size. This method is especially susceptible to increases in vegetation fraction due to liquid water in vegetation that pulls the 1030 nm ice absorption feature toward shorter wavelengths (Painter et al., 2003). In the MEMSCAG (multiple endmember snow-covered area and grain size) model grain size retrievals were accurate for snow fractions greater than 50% for 50-μm grain sizes and only greater than 90% for 1000-μm grain size (Painter et al., 2003). The susceptibility to accurately measure grain size is is therefore dependent on both the amount of snow

cover in the pixel and the snow grain size (inaccuracies increasing for larger grains).

3.4 Data and Simulated Data

3.4.1 AVIRIS Flights

As part of a Nevada EPSCoR Project, AVIRIS data were collected along the entire Sierra Nevada mountain range extending from north of Lake Tahoe to south of Mt. Whitney during the 2015 and 2016 snow-covered season (AVIRIS Data Portal, 2016). Data were acquired on four days: 2/24/15 during a very low snow year, 3/24/16 near maximum snow accumulation, and 5/12/16 and 5/18/16 during snow ablation and snow loss. The AVIRIS dataset used in this experiment consists of 224 contiguous spectral channels with wavelengths ranging 400-2500 nm and spectral bandwidth of approximately 10 nm at a nominal 15 m spatial pixel resolution. The HyspIRI Campaign's Level 2 processing pipeline transformed calibrated AVIRIS radiance data into surface reflectance using the Atmosphere Removal Algorithm developed by Gao et al. (1993) by modeling the absorption due to water vapor, carbon dioxide, ozone, nitrous oxide, carbon monoxide, methane, and oxygen as described in Thompson et al. (2015). Several channels were masked due to atmospheric correction artifacts [99-111 (1273-1393 nm); 150-177 (1782-2028 nm)] for a total of 183 channels used in this study.

3.4.2 Current Snow Mapping Products

The MODIS instrument contains 20 optical channels and is comprised of seven land reflectance bands with bandwidth and spatial resolution shown in **Table 3.1** (Barnes et al., 1998). The grain size retrieval algorithm for MODSCAG uses libraries of snow endmembers that were generated with model calculations of snow reflectance spectra for monodispersions of spheres of radii 10-1100 μm (10 μm intervals) and solar zenith angles ranging from 0° to 85° (Painter et al., 2009). The MODSCAG algorithm has a spatial resolution of 500 m (Painter et al., 2009).

Band	Bandwidth(μm)	Spatial Resolution (m)
1	0.620-0.670	250
2	0.841-0.876	250
3	0.459-0.479	500
4	0.545-0.565	500
5	1.230-1.250	500
6	1.628-1.652	500
7	2.105-2.155	500

Table 3.1: Spectral bandwidths and spatial resolution of the seven land reflectance bands for MODIS. In order to incorporate all bands the MODSCAG snow cover data product is only available at 500 m.

The Airborne Snow Observatory collects data with an ITRES CASI-1500 imaging spectrometer with a range from 365 to 1050 nm with ∼10 nm resolution for a total of 72 spectral bands (Painter et al., 2016). The grain size retrieval algorithm for ASO is modelled after the method of *Nolin and Dozier* (2000). However, this does not cover the entire 1030 nm absorption feature used in snow grain size estimates (Painter et al., 2013). Modeling broadband snow albedo past this feature where absorption depends on grain size must be extrapolated (Bair et al., 2016). The spatial resolution for CASI products is very fine at 3 m spatial pixel resolution (Painter et al., 2016). An even smaller spatial pixel resolution of 1.5 m is available, but the uncertainty in location for CASI snow depth is 1.5 m (Painter et al., 2016). ASO does not make use of NDSI to calculate snow-covered area, but instead uses lidar and snow-off vs snow-on gridded surfaces to determine snow depth and snow cover extent (Painter et al., 2016).

We explore the differences of AVIRIS, CASI, and MODIS in regards to fSCA and grain size approximations. EnMAP and HISUI will both have a satellite-based hyperspectral imager similar to AVIRIS (Guanter, et al., 2015; Matsunaga, et al., 2016). We provide a short summary of the spatial, spectral, and temporal resolutions of AVIRIS, CASI, MODIS, and the planned EnMAP, HISUI, and HyspIRI IS systems **Table 3.2**. To help visualize the differences in spectral resolution, **Figure 3.1** depicts three sample spectra from our masked AVIRIS flight line data overlayed with the

MODIS bandpasses and limited spectral range of CASI.

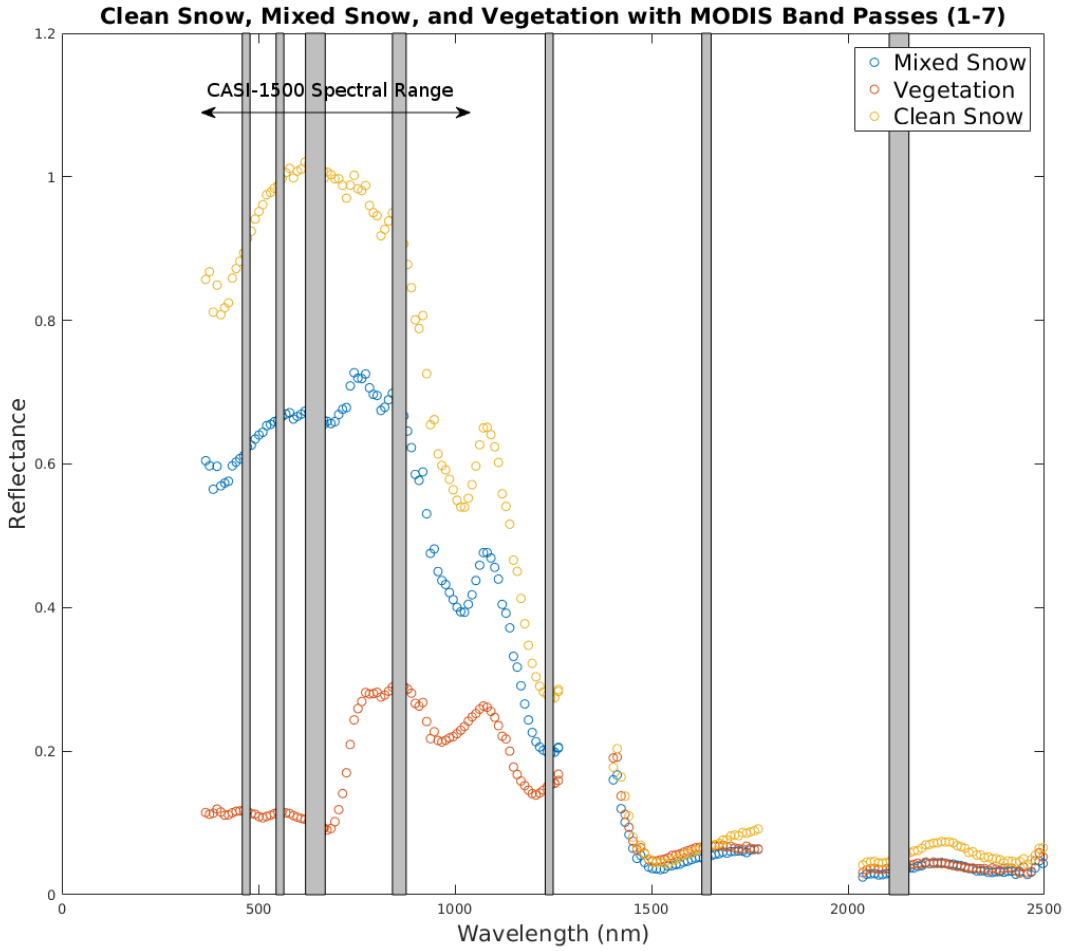

Figure 3.1: Clean snow, mixed snow, and vegetation of our true AVIRIS data plotted with MODIS band passes (1-7) with the limited spectral range of CASI-1500.

3.4.3 Simulated MODSCAG, CASI, EnMAP, and beyond

As described in Chapter 2, the algorithm and methods we have produced is based on previous work (MEMSCAG and MODSCAG) (Painter et al., 2003; Painter et al., 2009). Since the computational framework is nearly the same, in order to simulate the MODIS satellite, or any other satellite, we can take the much finer spectral resolution as well as the finer spatial resolution of AVIRIS to produce simulated

IS System	Spatial	Spectral	Temporal
AVIRIS (Green et al., 1998)	15 m	224 Bands 400-2500 nm Range ∼10 nm Resolution	*
CASI-1500 (Painter et al., 2016)	3 m	72 Bands 380-1050 nm Range ∼10 nm Resolution	*
MODIS (MODSCAG) (Painter et al., 2009)	500 m	**Table 3.1**	∼daily
EnMAP (Guanter et al., 2015)	30 m	185 Bands 420-1000 nm Range 900-2450 nm Range 6.5-10 nm Resolution	∼4 days
HyspIRI (Lee et al., 2015)	30 m	212 Bands 380-2500 nm Range 10 nm Resolution	16 days
HISUI (Matsunaga et al., 2016)	30 m	185 Bands 400-2500 nm Range 10-12.5 nm Resolution	∼3-4 times a month

Table 3.2: Summary is based on the current spatial, spectral, and temporal resolutions for snow mapping products available.

products based on varying spectral or spatial scales. In the example of MODIS, we take the relative spectral response functions of the MODIS bands (see **Table 3.1**) and using the AVIRIS channels that cover the MODIS bandpasses, convolve the bandpasses to the channels for each endmember in our library. We then aggregate the reflectances to varying spatial resolutions, and then perform our spectral mixture analysis across our sample selection that is now at lower MODIS spectral resolution. As long as the spectral resolution and spatial resolution of the satellite are known, the potential to simulate any satellite that is lower spectral or lower spatial resolution than AVIRIS is possible. While the specifics of EnMAP's spectral channels is not entirely known, it will certainly be similar to AVIRIS (see **Table 3.2**). We can simply aggregate pixel reflectances to 30 m resolution before performing spectral mixture analysis. In the example of CASI, which is at a higher spatial resolution, we may only compare the spectral resolution from our AVIRIS data interpolated to CASI

channels. CASI grain size calculations do not cover the entire 1030 nm absorption feature (Painter et al., 2013). However at ∼15 m resolution AVIRIS may not readily determine clear snow. In order to make a valid comparison of grain size we set a high NDSI > 0.9 threshold and look at pixel grain size based on the method provided by CASI compared to AVIRIS spectral channels (Painter et al, 2013). The workflow to produce our different snow product comparisons was described in detail in Chapter 2 (**Figure 2.1**).

Validation with true MODSCAG data is still an important future step, but our use of a self consistent data set provides an estimate of where the MODSCAG algorithm may not be performing well. We assume that a comparison between a simulated MODSCAG product and our AVIRIS data is valid for a multitude of reasons: (1) There is no difference in instrument noise and reflectance correction parameters, and thus by using normalized reflectance values across our AVIRIS model and simulated MODSCAG we eliminate any adverse effects of varying reflectances (2) Since the pixel aggregate is based on the nearly nadir viewing geometries of the same AVIRIS scene we eliminate any differences of off-nadir tilt, and due to the ephemeral nature of snow we assure that each scene comparison is using the same snow cover, a proxy for analysis on the same day. (3) Endmember selection and algorithm procedure is the same, and only spectrally different based on the spectral sampling of MODIS. This validation is applicable to any variation in simulated satellite selection of lower spectral and spatial resolution than AVIRIS.

We derive snow cover and grain size using a multiple endmember unmixing model that first tests for snow abundance and vegetation using NDSI and NDVI metrics at the full AVIRIS spatial and spectral resolution. Next, we present comparisons of simulated fSCA and grain size retrieval products (MODSCAG, CASI, EnMAP) containing the Sagehen Creek watershed with validation datasets from AVIRIS. While our methodology differs from the true MODSCAG or CASI products, consistency between our model and simulated products ensures that we are truly testing the influence of varying spectral and spatial resolutions on derived fSCA and grain size.

The following snow products were explored:

1. Simulated MODSCAG by aggregating AVIRIS reflectance data to 500 m. Then convolving pixels and endmembers to MODIS band centers from the MODIS (Aqua) relative spectral response (RSR). Followed by spectral mixture analysis.

2. Simulated EnMAP by aggregating AVIRIS reflectance data to 30 m, keeping the full spectral resolution. Followed by spectral mixture analysis.

3. Hypothetical grain size retrievals similar to CASI for pixels at NDSI > 0.9 (Painter et al., 2013).

3.5 Model Description

Our model and algorithm is based on MEMSCAG (multiple endmember snow-covered area and grain size) that was derived from MESMA (Painter et al., 2003; Robert et al., 1998). Our model simultaneously derives fSCA and snow grain size from a constrained linear spectral mixture analysis and is described in detail in Chapter 2. Unlike MEMSCAG which is coupled with its own radiative transfer model and in situ measurements, we have produced our own endmember library.

3.5.1 Library Endmembers

We interpolate snow endmembers from the Snow, Ice, and Aerosol Radiation (SNICAR) model available online at the University of Michigan (**Figure 2.2** ; Flanner et al. 2007; 2009).

Among many other parameters, the SNICAR model allows for snow grain sizes ranging from 30-1500 microns. Since MODSCAG makes use of a snow endmember library from 10-1100 microns at 10 micrometer intervals we too develop a snow endmember library of similar caliber for each of our AVIRIS scenes. The AVIRIS flights provide the solar elevation angle. From solar elevation angle we input a solar zenith angle as a parameter into the SNICAR model and produce varying snow grain sizes from 30 to 1100 micrometers at 10 micrometer intervals (**Figure 2.3**).

Vegetation, rock, soil, etc. endmembers were measured in situ in the region of Sage Hen. However, we opted to not use these measurements as the local vegetation species and mineralogy changes throughout the entire Sierra Nevada region. We therefore produced a generalized endmember library for typical vegetation and minerals/soils found in the Sierra Nevada. We interpolated and convolved vegetation, rock, soil, etc. endmembers from the USGS Spectral Library Version 7 [Kokaly et al., 2017] and from the ASTER Spectral Library Version 2.0 [Baldridge et al., 2009] to AVIRIS channels (**Figure 2.4** and **Figure 2.5**). Spectra that were sampled at a spectral resolution finer than AVIRIS were convolved to the AVIRIS channels with a Gaussian bandpass filter (Painter et al., 2003). As noted in section 3.4.1, spectral channels were masked where there were high atmospheric correction artifacts present in our data (around 1400 and 1900 nm). This model does not attempt to identify vegetation species or rock/soil mineralogy, so attention to specific bidirectional reflectance is not necessary and assumed nadir (Painter et al., 2003).

Of the endmembers chosen, preliminary spectral mixture analysis of the Sage Hen study site indicated that over 90% of mixed pixels were attributed to vegetation endmembers, and 100% of mixed pixels were attributed to only 10 endmembers (of a 26 total) outside of our snow endmembers. Therefore, to improve on computation times, we reduced the non-snow library to these 10 endmembers. It will be necessary to to do full library inversions at spatially random intervals throughout an entire flight line in the future to decide how valid this reduction is. **Figure 3.2** describes the vegetation, rock, soil, etc. endmembers used in spectral mixture analysis (excluding the 108 snow endmembers, which are shown in **Figure 2.3**).

3.5.2 Spectral Mixture Analysis

Our spectral mixture analysis is primarily based on previous work (Painter et al., 1998; Nolin and Dozier 2000; Painter et al., 2003; Painter et al., 2009). The spectral mixture analysis is based on equation (3.1), above. Solving this equation for the error provides us with the residuals, and to measure the spectrum-wide quality of fit we

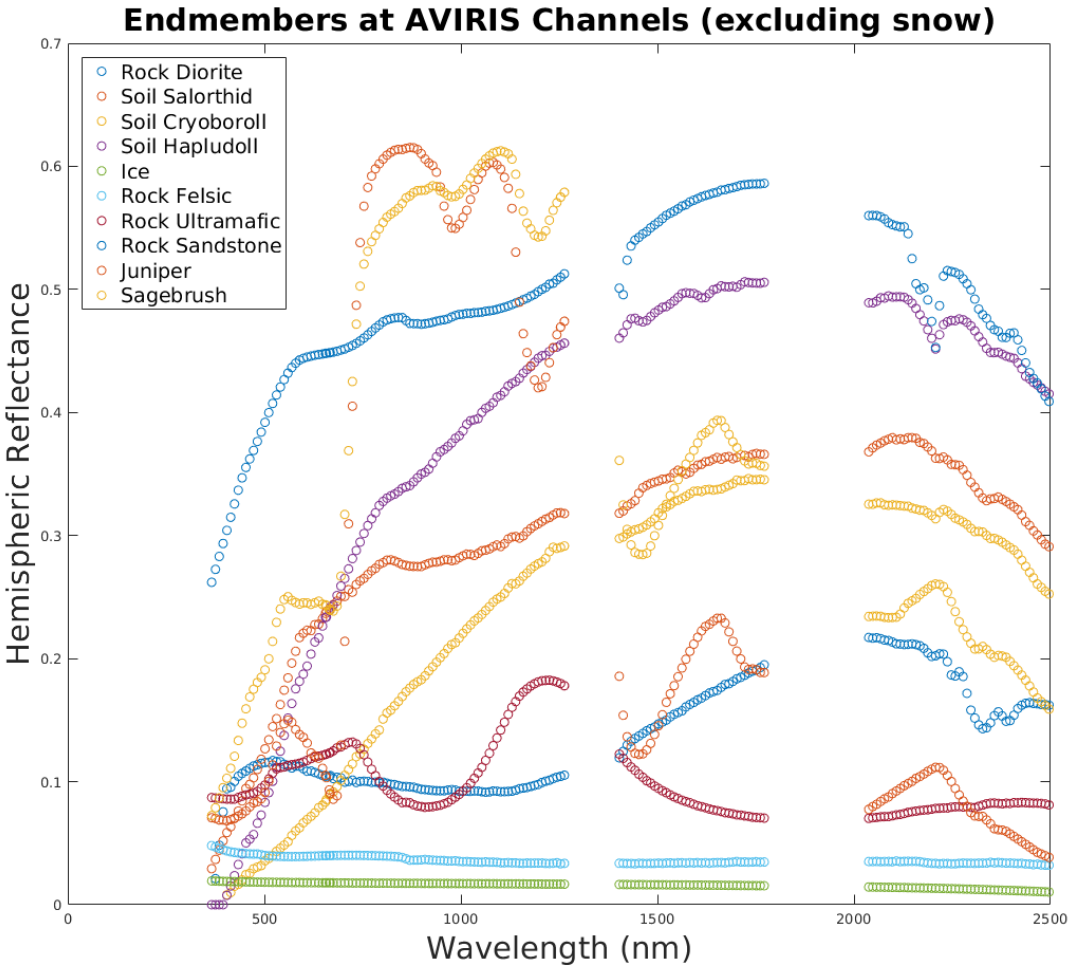

Figure 3.2: Vegetation, rock, soil, etc. endmembers convolved / interpolated to AVIRIS channels. These are the final ten endmembers used in our spectral mixture analysis emerging from preliminary analysis of the Sage Hen. Gaps in the spectra represent areas where atmospheric effects in original AVIRIS data exist and are subsequently masked.

average the root mean squared error (RMSE):

$$RMSE = [M^{-1} \sum_{c=1}^{M} E_c^2]^{1/2} \tag{3.2}$$

M is the number of AVIRIS bands in the spectral mixture analysis. The fraction endmembers are determined in the overdetermined case. The estimation of subpixel snow-covered area is derived from the shade-normalized snow fraction.

$$f_s = \frac{F_s}{\sum_{p \in s,v,r} F_p} = \frac{F_s}{1 - F_{shade}} \tag{3.3}$$

F_s is the snow spectral fraction, F_p are the physical spectral fractions snow, vegetation, rock, etc. By normalizing the additive complement of the shade fraction topographic effects of shadowing and illumination are accounted for (Adams et al., 1993; Painter, 1998; Painter et al., 2003).

MODSCAG includes the following constraints: (a) a model is considered valid if fractions are in the range [-0.01,1.01] (b) overall RMSE $< 2.5\%$, and (c) no three spectrally consecutive residuals exceed 2.5%. Pixels outside of these constraints are modeled more loosely with the following constraints: (a) [-1.01,2.01] (b) overall RMSE $< 5\%$, and (c) no three spectrally consecutive residual exceed 5%. The estimation of subpixel snow-covered area is derived from the shade-normalized snow fraction (Painter et al., 2009).

We attempted to replicate the MODSCAG model, and through optimization and sensitivity studies our model includes the following constraints: (a) a model is considered valid if fractions are in the range [-0.01,1.01] and sum to 1.0 (b) overall RMSE is <2% for 2-endmember solutions (i.e. snow and shade only) but overall RMSE is <5% for all other combinations, and (c) we ignore spectrally consecutive residual constraints.

Additionally, we only perform spectral mixture analysis on any pixel whose NDSI > 0.0. The NDSI threshold improves computation times instead of looking at each pixel, and since spectral mixture analysis is only accurate down to 15% snow cover the given NDSI threshold threshold includes this region in all endmember combination cases (Rittger et al., 2013). Additionally, we include a NDVI > 0.2 threshold check to ignore 2-endmember solutions and immediately move on to 3 or more endmember solutions to improve computation time since snow has a low $\sim$0.1 NDVI value. The model also reduces computation times by dividing the spectral mixture analysis into two runs. Since the number of snow endmembers is 108 (30-1100 at 10 μm intervals) each n-choose-k problem is on the order of 108 endmembers plus 10 non-snow

endmembers. Instead, we divide the snow endmembers into a preliminary grouping using a coarse grain size step and then a final grouping using a finer snow grain size step based on the results of the first spectral mixture analysis run. The first spectral mixture analysis looks at a smaller subset of snow endmembers (100-1100 at 100 μm intervals) for a total of 11 snow and 10 non-snow endmembers. From this first run, the selection is narrowed further in the second run to snow endmembers that vary from the 10 μm intervals before and after the chosen endmember. For example, a pixel will first look at the 11 snow and 10 non-snow endmembers, and might choose an n-endmember combination that uses the 200 μm grain size snow endmember. Then, on the second run, the snow endmembers that are the new input parameters to the spectral mixture analysis range from 110-290 μm at 10 μm intervals. Since our preliminary results have shown reasonably low scene-wide RMSE, we currently set the model to a maximum of 4-endmember combinations. The workflow of our spectral mixture analysis is summarized in Chapter 2 (**Figure 2.11**).

3.6 Sensitivity Study

We performed a synthetic study to understand the sensitivity of our model's ability to determine fSCA and grain size for varying snow grain sizes at different endmembers [Painter et al., 2003]. While we generated synthetic hyperspectral scenes for all endmembers, **Figures 3.2 and 3.3** show the sensitivity analysis for one common endmember that was also the largest source of error, vegetation (juniper) with a snow grain size of 700 μm. All other synthetic endmember scenes had a lower error. The simulated scene is a linear combination summing to 100% of a single snow grain size endmember and the vegetation endmember varying from 0 to 100%, incremented by 1% mixtures. **Figure 3.3** depicts this combination for 10% increments.

Figure 3.4 shows that our model is accurate at determining fSCA percentage and true grain size for nearly all true snow cover percents and for varying snow grain sizes. It is important to note that for fSCA, we overestimate true snow cover percent between ~85-99%, but only by <15%. We highlight the discrepancy between shade-

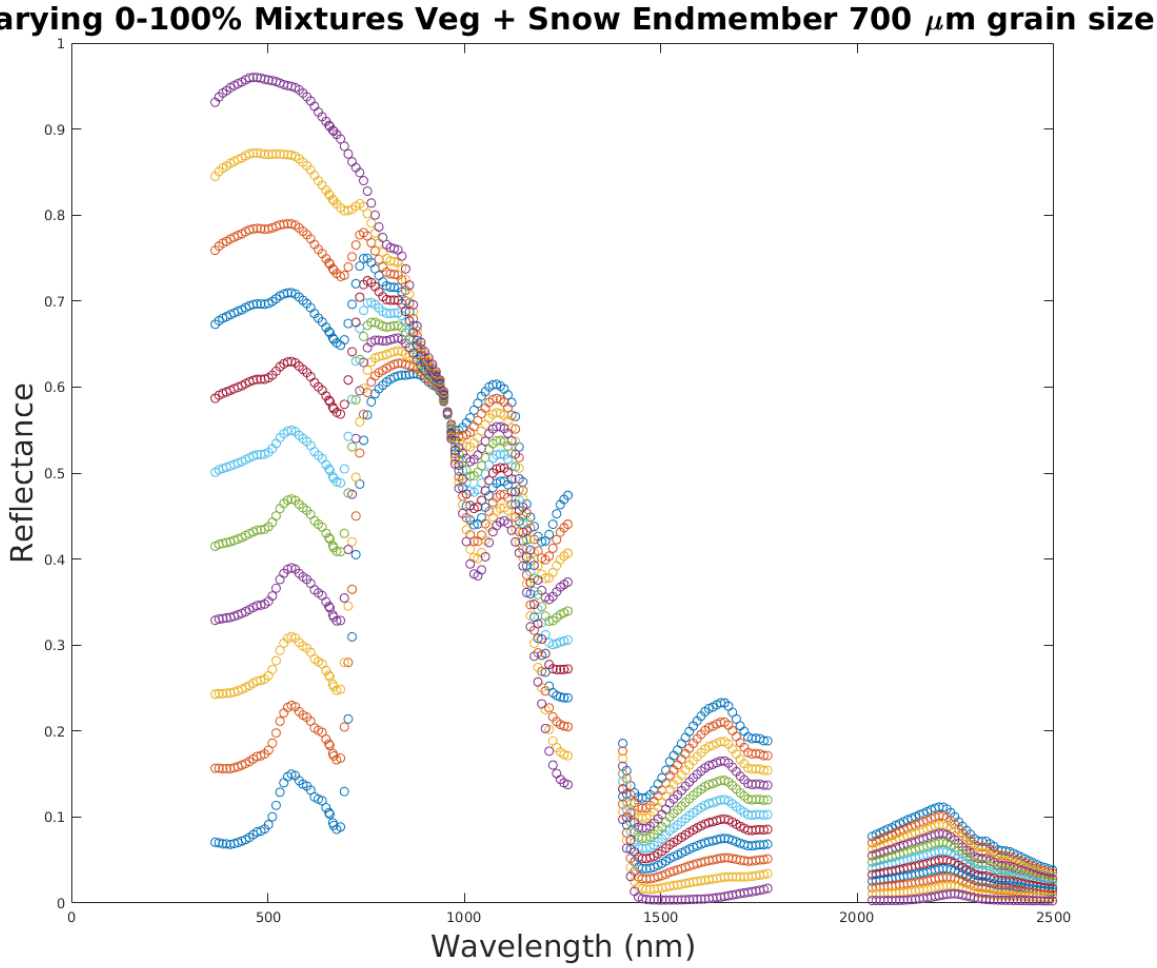

Figure 3.3: Example of synthetic spectral mixtures from the sensitivity study. Mixtures vary from 100% snow 0% vegetation to 0% snow 100% vegetation in 10% increments. Snow endmember shown is 700 μm grain size and vegetation endmember shown is juniper.

not-normalized '*' and shade-normalized 'O' (final product). Similarly, discrepancies in modelled grain size parallel discrepancies in fSCA. In all erroneous instances, grain size is underestimated. We find that these results are due to the model choosing the most parsimonious solution first. Since shade is an endmember always present, our model will determine a pixel is purely snow (combined with a shade endmember-equation 3) if that combination is below our 2% RMSE threshold, as opposed to a combination of snow and another endmember first. Therefore the model will prefer

a single snow endmember that is of a lower grain size combined with shade over the correct snow endmember combined with vegetation or comparatively whatever true endmember is present. This discrepancy is most exaggerated with vegetation endmembers. This is likely due to the liquid water in the vegetation that brings the characteristic 1030 nm ice absorption feature toward shorter wavelengths (Painter et al., 2003).

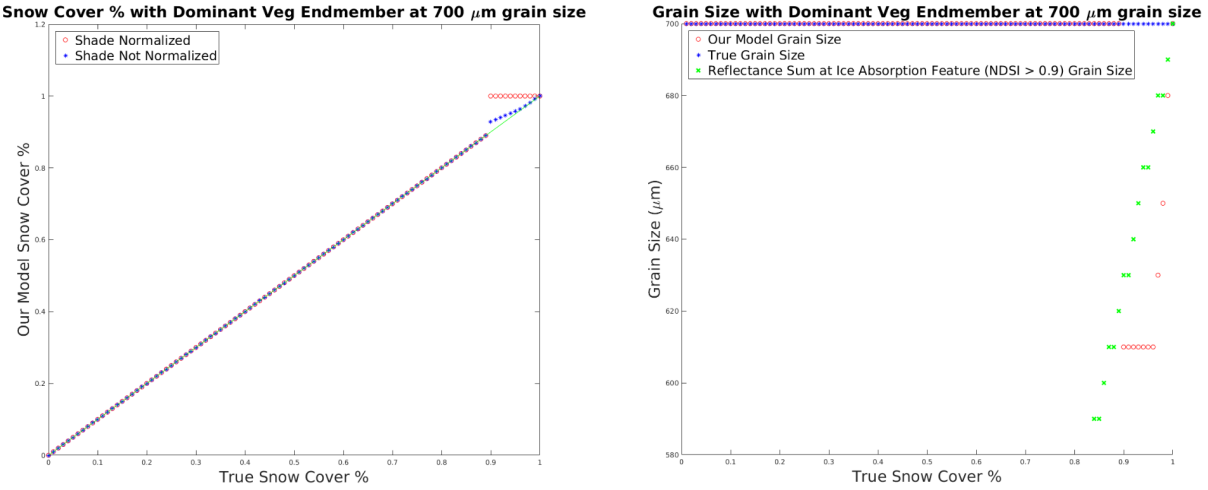

Figure 3.4: Synthetic sensitivity modeling results for 700 μm grain size for the optimized model.

3.7 Comparisons

We use AVIRIS data to compare fSCA and grain size retrievals to simulated MODSCAG and EnMAP products, and grain size retrievals similar to CASI (Painter et al., 2013; Painter et al., 2016). The details of simulated MODSCAG, EnMAP, and CASI retrieval methods are found within Section 3.4.3. The workflow that leads to these comparison products is summarized in Chapter 2 (**Figure 2.1**). As is common practice, we omit pixels with fSCA < 0.15 due to the erroneous spectral mixture of snow with other land covers at these percentages (Painter et al., 2009; Rittger et al., 2013).

3.7.1 Comparison Metrics

Three fractional metrics provide difference in per-pixel fSCA and grain size values: mean difference, median difference, and RMSE (Rittger et al., 2013). The RMSE is defined as:

$$RMSE = \sqrt{\frac{1}{N}\sum_{N}(f_{SCA}^{SimulatedProduct} - f_{SCA}^{AVIRIS})^2} \tag{3.4}$$

Where N is the number of pixels in the image that the simulated product (MODSCAG or EnMAP) or where aggregated AVIRIS pixels depict as snow. Similarly, these metrics are applied to grain size values in place of fSCA (equation 3.4). We avoid areas where both do not see snow, as including those pixels would give erroneously good RMSE values (Rittger et al., 2013). We also provide a scene-wide SCA comparison differencing the total SCA of the AVIRIS aggregates compared to our simulated products.

3.7.2 Comparison Statistics

Figure 3.5 depicts one of our validation AVIRIS 3/24/16 flight lines near maximum snow accumulation. Mean fSCA, RMSE, vegetation fraction, and grain size for the full scene are 0.4679, 0.0208, 0.2714, and 829.2 μm respectively. Due to the omission of pixels where fSCA is < 0.15 we also omit those pixels in the full scene. There are large patches of small grain sizes that are likely false (northwest corner and east). These features are classified as snow due to our low NDSI threshold of 0.0. If we set an NDSI threshold of 3.0, these densely vegetated regions are eliminated along with their erroneous grain sizes. Future work will address this issue with a higher NDSI threshold before all subsequent comparisons. Another discrepancy that is visible is the presence of a small ($\sim$10% or less) vegetation fraction in areas of pure snow (i.e. lakes). The source of this error is due to the snow in these areas containing contaminents that reduce the overall reflectance by $\sim$20%. With the overall reflectence reduced, the algorithm will not associate our endmembers that are pure snow to these

pixels without inclusion of lower reflectance endmembers. To fix this error we might include a dirty snow endmember at varying grain sizes in future analysis. Additionally, we provide visual fSCA and grain size comparisons of the same AVIRIS flight line aggregates with the simulated products in **Figure 3.6** for simulated MODSCAG and **Figure 3.7** for simulated EnMAP.

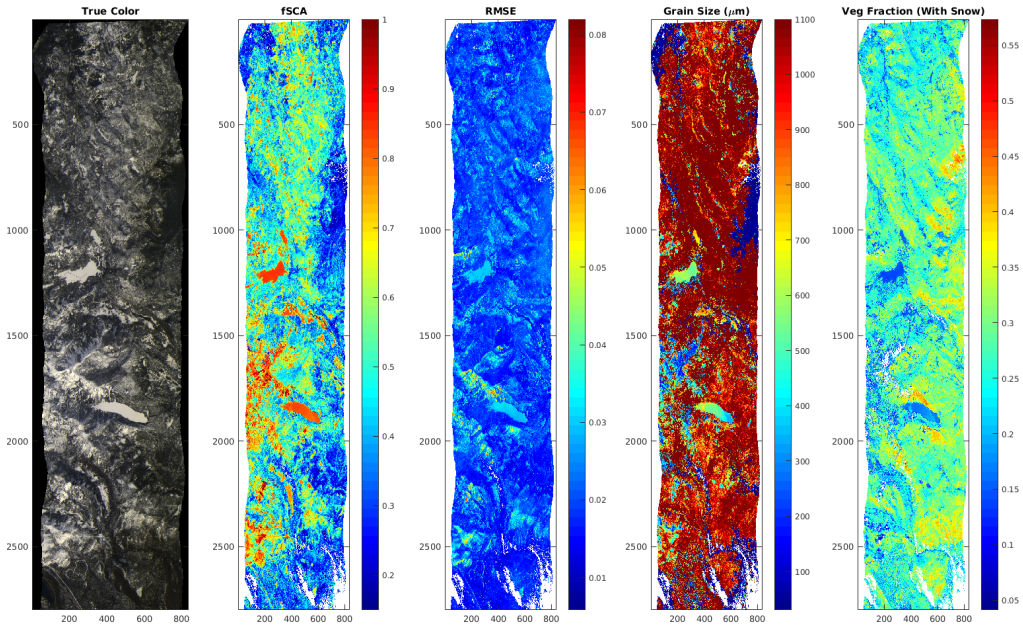

Figure 3.5: Validation AVIRIS flight line from 3/24/16. This flight line is the most abundant snow scene used in our comparison. Mean fSCA, RMSE, vegetation fraction, and grain size for the full scene are 0.4679, 0.0208, 0.2714, and 829.2 μm respectively. Additional flight lines available in the Appendix.

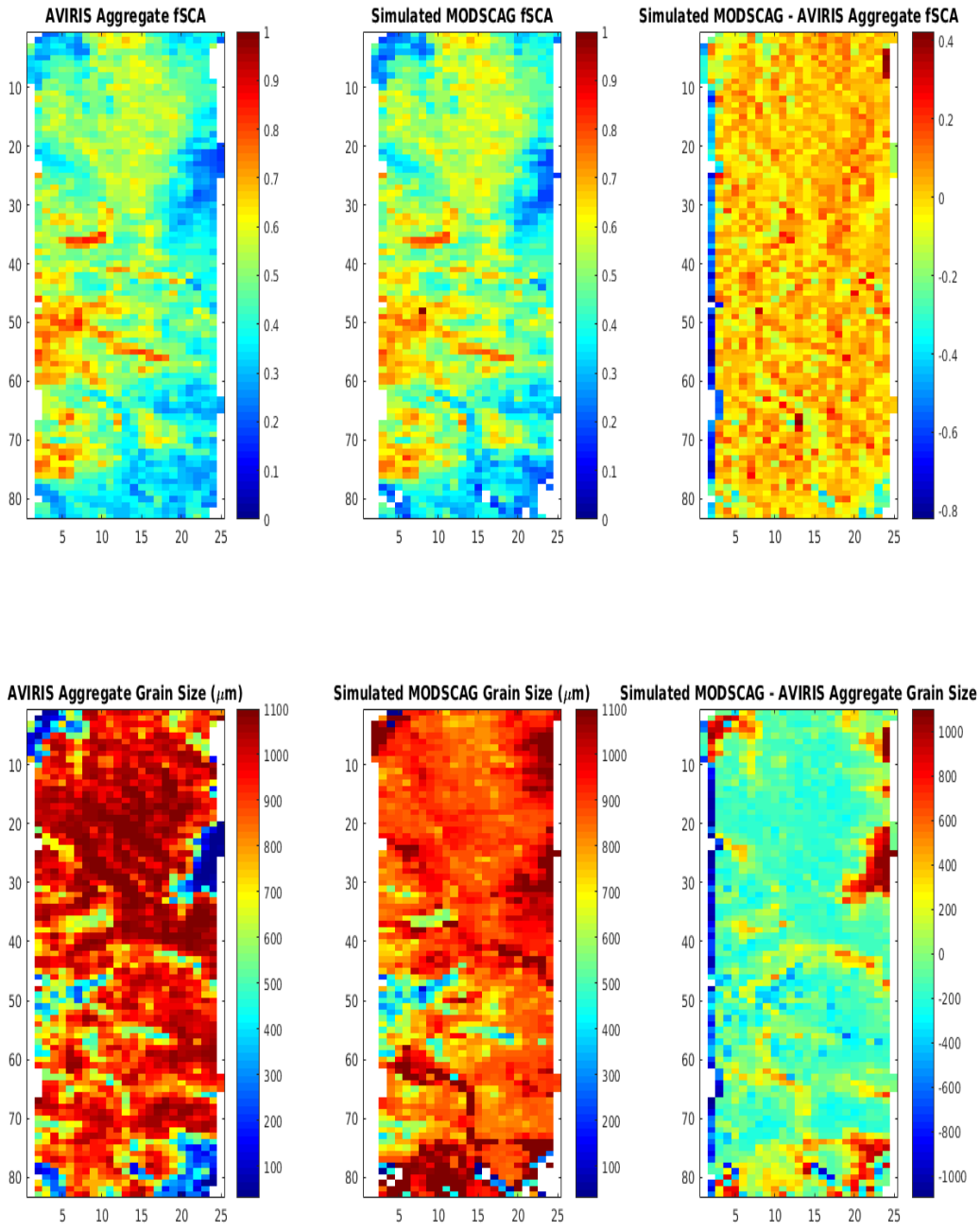

Figure 3.6: AVIRIS aggregate to 500 m resolution with associated fSCA and grain size compared with simulated MODSCAG with associated fSCA and grain size from 3/24/16. The third plots in each row represent the difference with masked pixels being exactly equivalent in value. Statistical differences between these two images are provided in **Table 3.3** and **Table 3.4**.

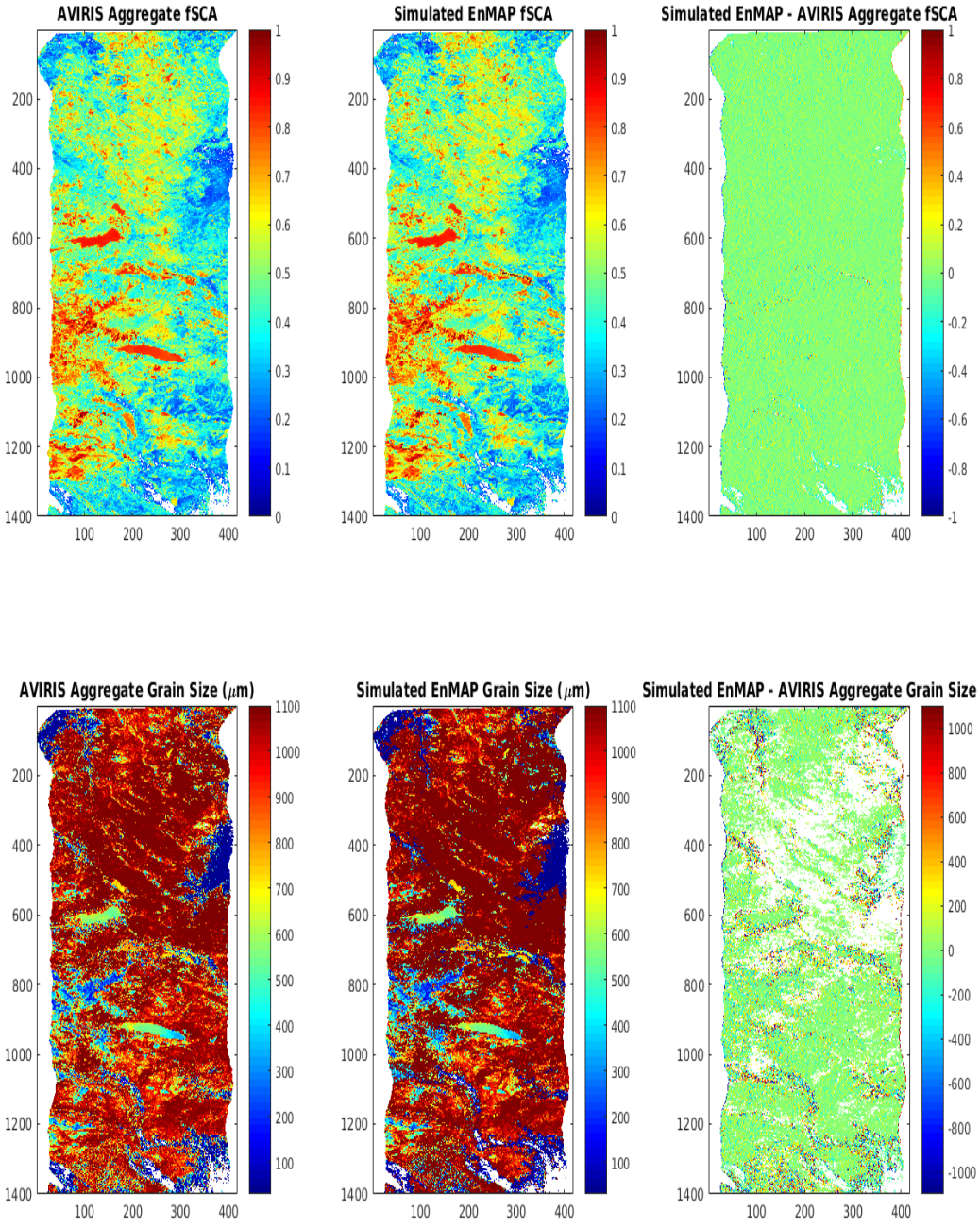

Figure 3.7: AVIRIS aggregate to 30 m resolution with associated fSCA and grain size compared with simulated EnMAP with associated fSCA and grain size from 3/24/16. The third plots in each row represent the difference with masked pixels being exactly equivalent in value. Statistical differences between these two images are provided in **Table 3.3** and **Table 3.4**.

Table 3.3 summarizes error matrix results for classification of snow pixels and total SCA results for our simulated MODSCAG and simulated EnMAP products. The table depicts how well our simulated products determine snow pixels compared to our true AVIRIS aggregates. As expected, commission (False Positive, FP) results, pixels where the simulated product determined snow and AVIRIS does not, are zero or less than ∼0.4%. Omission (False Negative, FN) results, pixels where the simulated product does not determine snow and AVIRIS does, is strikingly different between both products. In low snow (2/24/15 and 5/18/16) simulated MODSCAG produced high omission, 46% and 21% respectively, compared to <4% for all dates with simulated EnMAP. However, in abundant snow (3/24/16) MODSCAG FN results were ∼5%, compared to ∼1% with simulated EnMAP. Two binary statistics, sensitivity and accuracy, are included to elaborate on hit rate for snow pixels and the total scene (formulas in table). Accuracy results were all >95% for simulated EnMAP while accuracy results suffered significantly in low snow (2/24/15 and 5/18/16), 54% and 79% respectively, for simulated MODSCAG. We also include the percent difference in total SCA between the simulated product and the true AVIRIS scene. The percent difference describes the sum of the fSCA to emphasize total SCA of a scene as opposed to just binary snow/not snow. For low snow (2/24/15 and 5/18/16) simulated MODSCAG performs very poorly underestimating total SCA by -78% and -86% respectively compared to simulated EnMAP with -22% for both days. For abundant snow, the percent difference is notably different with both simulated MODSCAG and simulated EnMAP within 1% of total SCA.

The three fractional statistics for simulated MODSCAG and simulated EnMAP for the different study days are summarized in **Table 3.4**. As expected, over all the images, the RMSE for simulated MODSCAG fSCA is 0.2155 with a range of 0.1425-0.2566 and standard deviation of 0.0634, while the values are much lower for simulated EnMAP with an RMSE of 0.1599 a range of 0.1862-0.2072 and standard deviation of 0.0645. The median difference for simulated MODSCAG fSCA is -0.1561 with a range of -0.2418-0.0125 and standard deviation of 0.1460. Again, these values are

Date	Variable	Simulated MODSCAG	Simulated EnMAP
2/24/15 (low snow)	True Positive (TP) %	11.7	7.8
	False Positive (FP) %	0.0	0.9
	False Negative (FN) %	45.9	4.0
	True Negative (TN) %	42.4	87.3
	Sensitivity % TP/(TP+FN)	20.3	65.9
	Accuracy % (TP+TN)/(TP+FP+FN+TN)	54.1	95.1
	Total SCA (Percent Error)	-77.6	-21.9
3/24/16 (abundant snow)	True Positive (TP) %	87.0	86.1
	False Positive (FP) %	0.2	0.4
	False Negative (FN) %	5.0	0.9
	True Negative (TN) %	7.7	12.6
	Sensitivity % TP/(TP+FN)	94.6	99.0
	Accuracy % (TP+TN)/(TP+FP+FN+TN)	94.7	98.7
	Total SCA (Percent Error)	0.7	-0.2
5/18/16 (low snow)	True Positive (TP) %	2.6	2.3
	False Positive (FP) %	0.0	0.3
	False Negative (FN) %	21.0	1.2
	True Negative (TN) %	76.3	96.2
	Sensitivity % TP/(TP+FN)	10.9	65.2
	Accuracy % (TP+TN)/(TP+FP+FN+TN)	78.9	98.5
	Total SCA (Percent Error)	-86.5	-22.3

Table 3.3: Summary of error matrix results and total SCA percent difference for simulated snow products.

much lower for simulated EnMAP fSCA at -0.0412 with a range of -0.0623-(-0.0006) and standard deviation of 0.0352. Synonymous mean values are also summarized in **Table 3.4**. For the three flight lines, simulated MODSCAG underestimates fSCA in

low snow (2/24/15 and 5/18/16) and does quite well in abundant snow (3/24/16). EnMAP also underestimates fSCA in low snow, but to a much lesser extent than MODSCAG, is also more accurate in abundant snow.

Date	Variable	Statistic	Simulated MODSCAG	Simulated EnMAP
02/24/15 (low snow)	fSCA	RMSE	0.2566	0.2072
		Mean Difference	-0.2271	-0.0695
		Median Difference	-0.2391	-0.0608
	Grain Size (Overlap Only)	RMSE	233.8	293.8
		Mean Difference	167.9	4.025
		Median Difference	145.5	0
03/24/16 (abundant snow)	fSCA	RMSE	0.1425	0.0864
		Mean Difference	-0.0106	-0.0011
		Median Difference	-0.0125	-0.0006
	Grain Size (Overlap Only)	RMSE	269.8	216.0
		Mean Difference	-9.1	16.6
		Median Difference	-91.7	0
05/18/16 (low snow)	fSCA	RMSE	0.2474	0.1862
		Mean Difference	-0.2291	-0.0685
		Median Difference	-0.2418	-0.0623
	Grain Size (Overlap Only)	RMSE	261.0	322.4
		Mean Difference	147.7	5.534
		Median Difference	188.2	7.5
Average (all 3 days)	fSCA	RMSE	0.2155	0.1599
		Mean Difference	-0.1556	-0.0464
		Median Difference	-0.1561	-0.0412
	Grain Size (Overlap Only)	RMSE	254.9	277.4
		Mean Difference	102.2	8.7
		Median Difference	80.7	2.5

Table 3.4: Summary of fractional statistics for simulated scenes.

For grain size we focus on only the pixels where both the simulated product and

AVIRIS aggregates share snow cover. This ensures that our grain size comparison statistics are not skewed by pixels with missing snow as we are more interested in how grain size differs between our validation AVIRIS datasets. For simulated MODSCAG overall grain size RMSE is 254.9 with a range of 233.8-269.8 and standard deviation of 18.8. The mean difference for simulated MODSCAG grain size is 102.2 with a range of -9.1-167.9 and standard deviation of 96.9. The median difference for simulated MODSCAG grain size is 80.7 with a range of -91.7-188.2. For simulated EnMAP the overall grain size RMSE is 277.4, with a range of 216.0-322.4 and standard deviation of 55.1. The mean difference for simulated EnMAP grain size is 8.7 with a range of 4.0-16.6 and standard deviation of 6.9. The median difference for simulated EnMAP grain size is 2.5 with range 0-7.5 and standard deviation of 4.3. For the three flight lines, simulated MODSCAG over estimates grain size in low snow (2/24/15 and 5/18/16) and only slightly underestimates grain size in abundant snow (3/24/16). Despite very narrow normal distributions about 0 for mean/median differences and low overall mean and median differences EnMAP maintains a high overall RMSE for grain size. **Figures 3.8-3.10** are histogram plots for each flightline date that help visualize these fSCA and grain size comparison statistics. Due to the normality of the fSCA and grain size retrievals about the mean difference, presented in the histogram plots, we justify a simulated model comparison using the RMSE and mean difference parameters. We plot RMSE vs mean difference to visualize the improvements of the models based on simulation type (EnMAP or MODSCAG) and date **Figure 3.11**. Models closer to the origin are more accurate. The results indicate EnMAP is consistently more accurate at fSCA and grain size retrievals, especially in low snow.

Table 3.5 summarizes grain size retrieval methods and simulated CASI products similarly. We omit discussion of comparison statistics for the table, as the results for these grain size retrieval methods are inconsistent, and therefore we leave interpretations of these inconsistencies to the discussion section. **Figure 3.12** are histogram plots of **Table 3.5** similar to the histogram plots for our simulated products for the varying grain size retrieval methods as discussed in section 3.4.

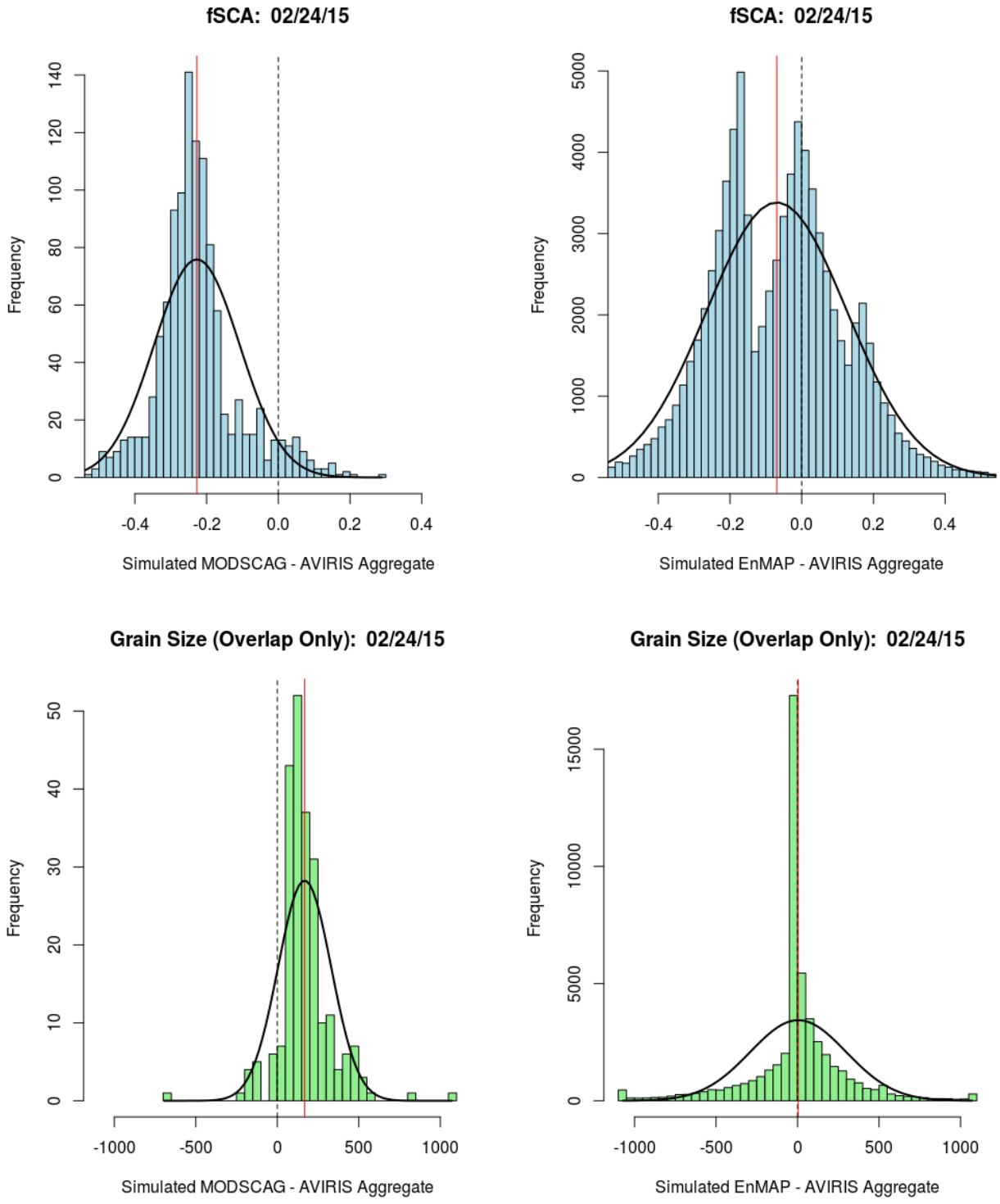

Figure 3.8: Histogram plots of comparison statistics for simulated MODSCAG (left) and simulated EnMAP (right) for 2/24/16 (low snow year).

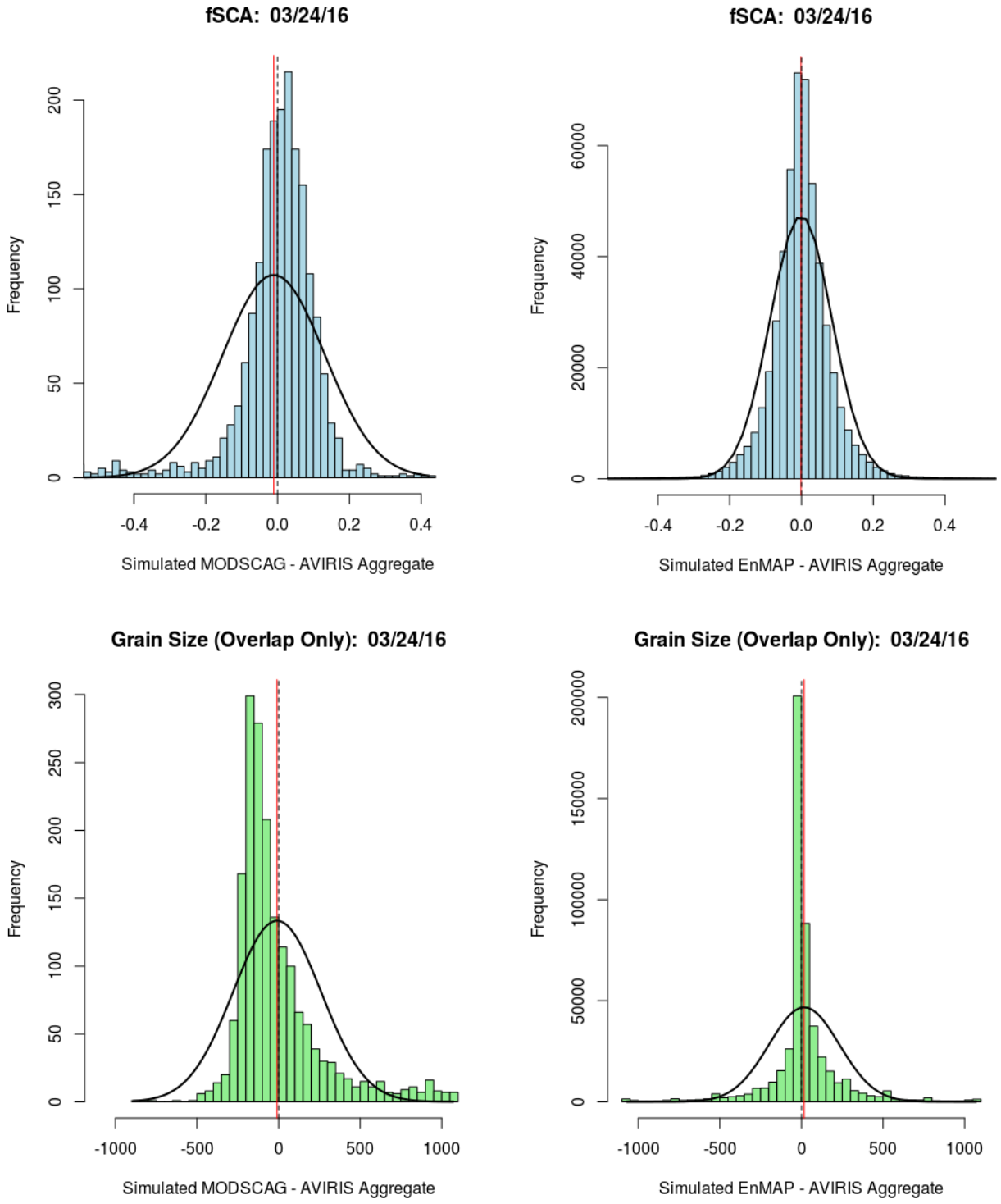

Figure 3.9: Histogram plots of comparison statistics for simulated MODSCAG (left) and simulated EnMAP (right) for 3/24/16 (maximum snow accumulation).

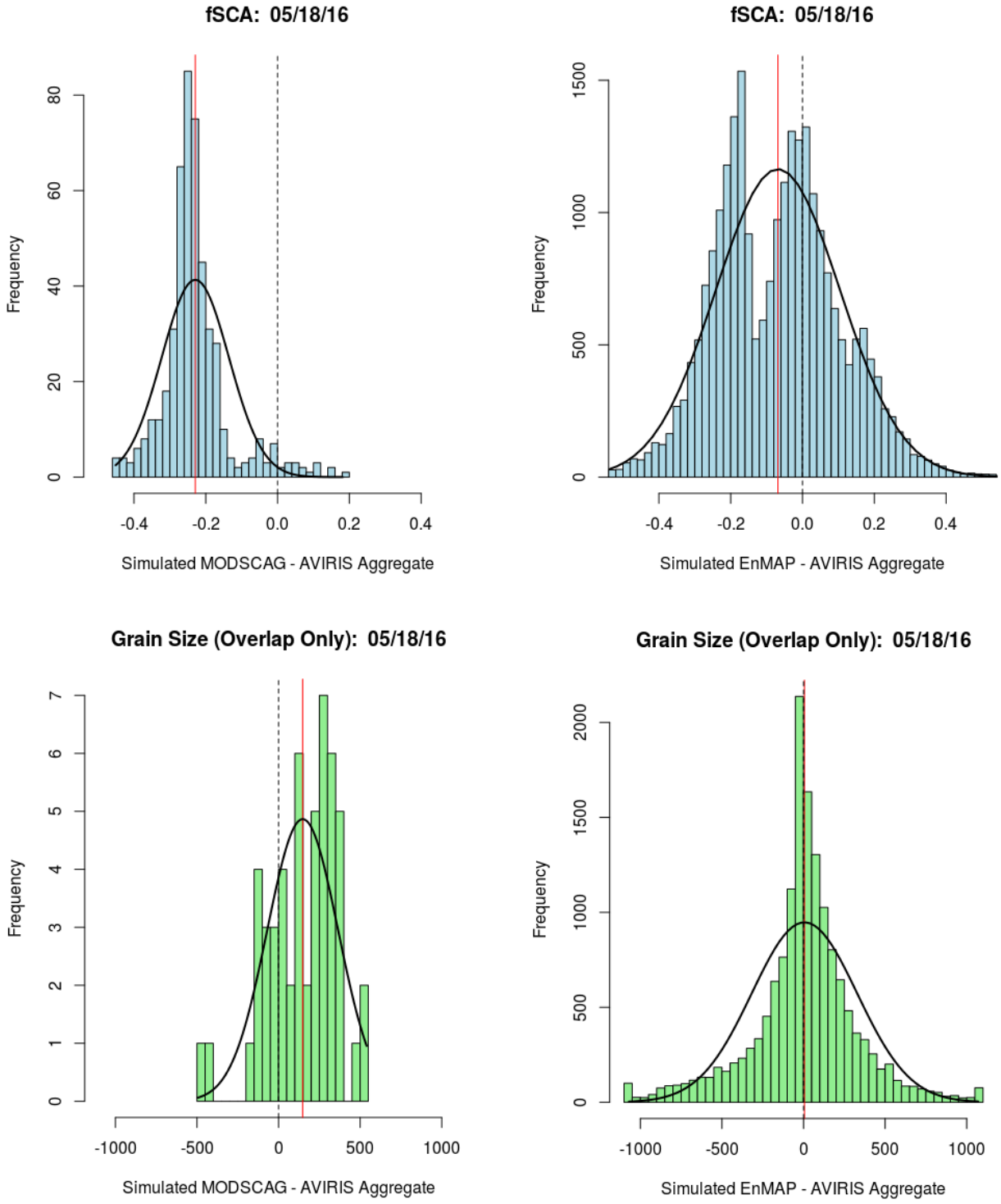

Figure 3.10: Histogram plots of comparison statistics for simulated MODSCAG (left) and simulated EnMAP (right) for 5/18/16 (snow ablation and snow loss).

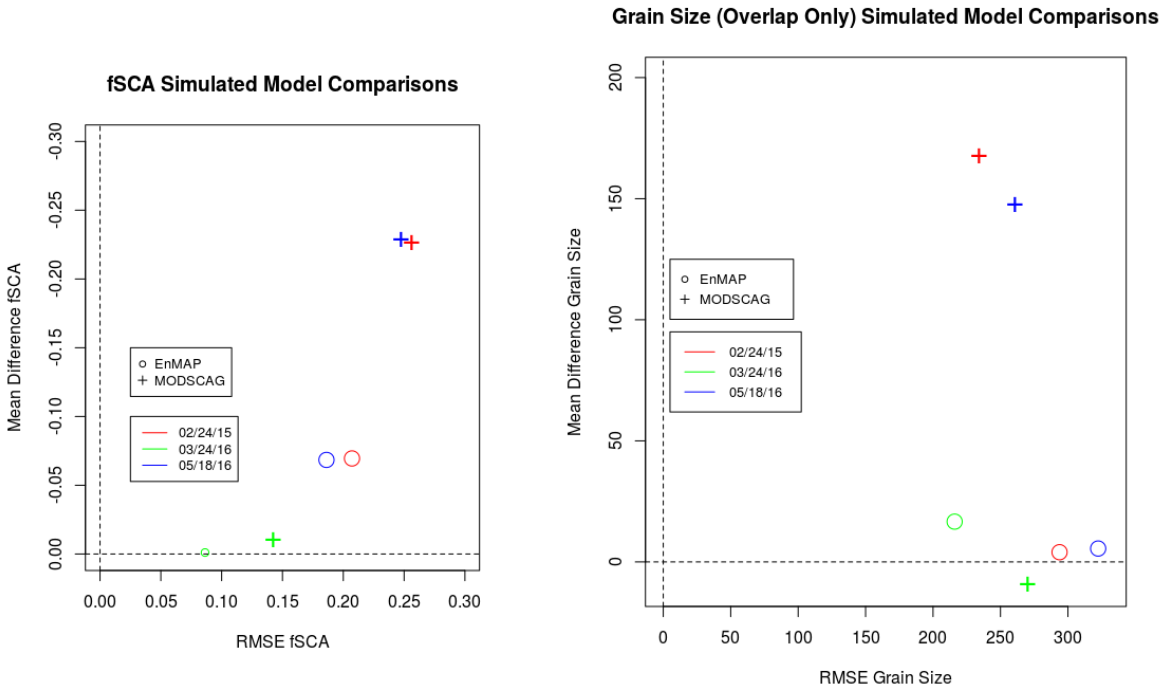

Figure 3.11: Simulated model comparisons for both fSCA and grain size retrievals. Models closer to the origin are more accurate. The results indicate EnMAP is consistently more accurate at fSCA and grain size retrievals, especially in low snow (02/24/15 and 05/18/16).

3.8 Discussion

Our study highlights the significant effects of not only the spatial resolution, but also the spectral resolution on fSCA and grain size retrievals. Recall that fSCA values should range from 0 to 1, with a RMSE or mean/median difference of 0 meaning the model provides 100% accurate fit to true snow cover. For simulated MODSCAG, the average of both low snow scenes (2/24/15 and 5/18/16) fSCA RMSE is 0.2520 with a -0.2281 mean and -0.2405 median difference. Additionally, omission (FN) was 33.5% and average accuracy was 66.5%. Our simulated EnMAP product for the same low snow scene show significant improvement over the simulated MODSCAG result. Average fSCA RMSE was 0.1967 with a -0.0690 mean and -0.0612 median difference. Additionally, omission (FN) was 2.6% and average accuracy was 96.8%. These drastic differences were also noticeable in the total SCA percent error. Taking

Date	Variable	Statistic	(AVIRIS channels)*	Simulated CASI	AVIRIS - CASI
02/24/15 (low snow)	Grain Size (Overlap Only)	RMSE	185.6	192.0	25.5
		Mean Difference	61.8	56.8	-5.00
		Median Difference	0	0	0
03/24/16 (abundant snow)	Grain Size (Overlap Only)	RMSE	224.4	96.6	156.8
		Mean Difference	-195.7	-53.3	142.3
		Median Difference	-170.0	-40.0	140.0
05/18/16 (low snow)	Grain Size (Overlap Only)	RMSE	229.0	237.1	115.4
		Mean Difference	110.6	181.4	70.8
		Median Difference	140.0	190.0	0
All	Grain Size (Overlap Only)	RMSE	213.0	175.2	99.2
		Mean Difference	-7.8	61.6	69.4
		Median Difference	-10	50	46.7

Table 3.5: Summary of comparison statistics for AVIRIS and CASI grain size retrieval methods. * Denotes the Reflectance Band Feature Method used for pixels where NDSI > 0.9 explained in section 3.4 (Painter et al., 2013).

the average of both low snow scenes (2/24/15 and 5/18/16) we find simulated MODSCAG produced a -82% error from the true total AVIRIS SCA as opposed to -22% for simulated EnMAP. That is a 73% improvement in total true SCA. In contrast, simulated MODSCAG fSCA retrievals worked well in abundant snow (3/24/16). The fSCA RMSE was only 0.1425 with a mean and median difference of $\sim$0.01. Additionally, FN was only 5% and total accuracy was 94.7% Simulated EnMAP fSCA RMSE was 0.0864 and total accuracy was 98.7%. This is nearly a 65% increase in fSCA RMSE, but both products do an excellent job of discriminating snow. In total, Simulated EnMAP products showed an improvement in RMSE fSCA calculations over our simulated MODSCAG product by $\sim$35%. These improvements are likely related to the enhanced spatial resolution, but also higher spectral resolution as well. We should expect to see such additional improvements when using actual EnMAP data to model snow properties.

Both simulated EnMAP and simulated MODSCAG share large grain size RMSE values between 200-300 μm. However, simulated EnMAP improves at getting to the correct grain size, as the mean/median difference values for simulated EnMAP

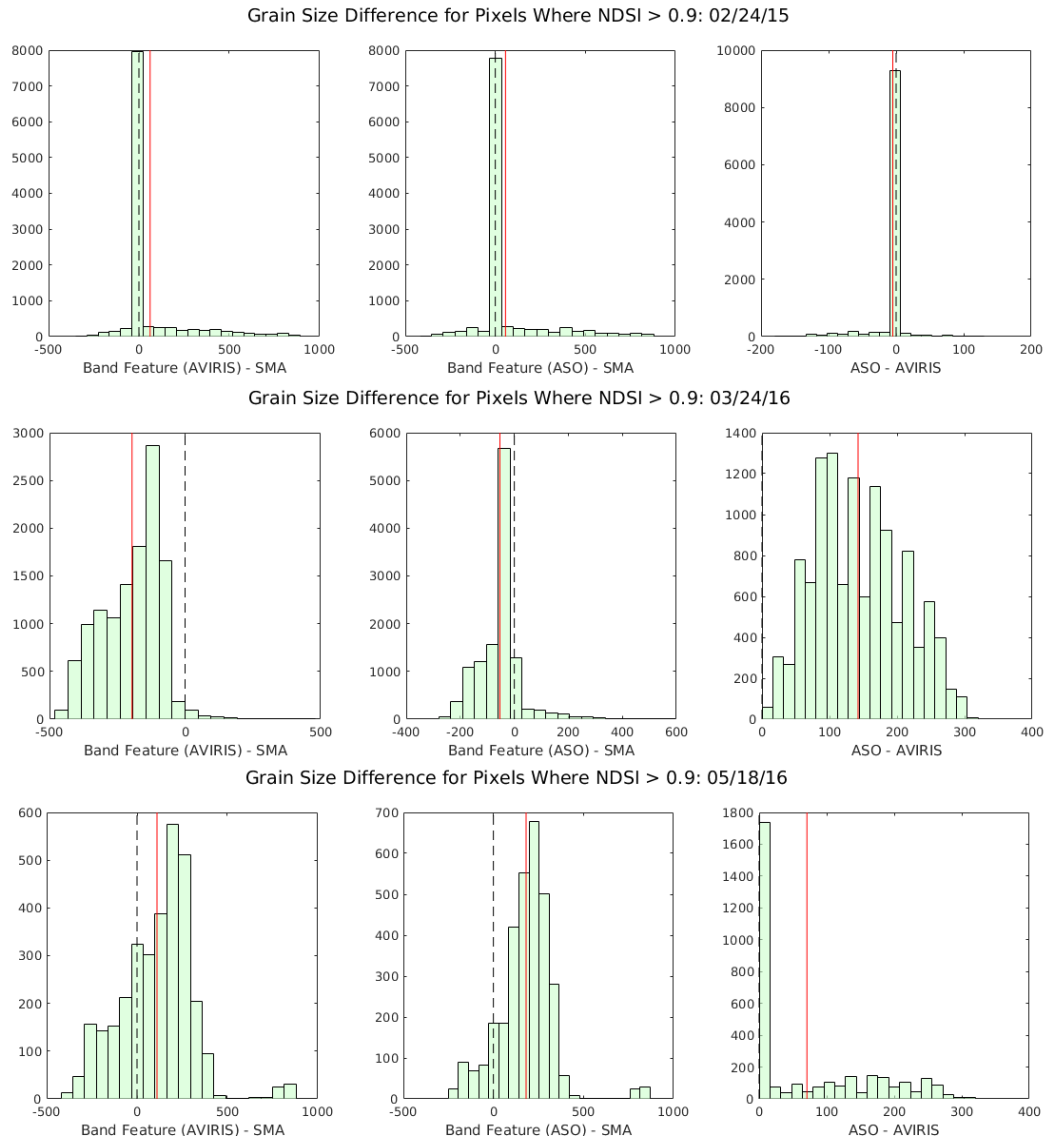

Figure 3.12: Histogram plots of comparison statistics for grain size retrieval methods. Grain Size retrieval methods explained in Section 3.4.

are consistently near zero, meaning a very good fit to the actual grain size. The simulated EnMAP increased grain size precision is likely related to the improvement in spectral resolution. Multispectral and hyperspectral satellite systems that solve the constrained least squares problem to determine fSCA and grain size (equation 3.1) rely on a system of equations equivalent to the number of bands/channels used. The additional spectral resolution provides a solution that takes advantage of finer spectral detail. Improved spectral detail across a wide range of wavelengths should have the

effect of improving unmixing algorithms. However, the more alike endmembers are in certain regions and specifically if the regions chosen are similar input parameters for the spectral mixture analysis, like the liquid water in vegetation that brings the characteristic 1030 nm ice absorption feature toward shorter wavelengths, may lead to inabilities to provide enough discrepancy between endmembers if they are similar throughout the channels used. Vegetation also has a large decrease in reflectance beyond ∼1000 nm, similar to snow, so the water in vegetation may masquerade as a larger grain size. We note that this difficulty to accurately replicate the grain size at each pixel for EnMAP compared to the AVIRIS aggregate is likely due to this effect and is probably the source of the strong outliers that drive the RMSE in grain size higher, but we also suggest others. Our selected flight lines for this study cover the Sage Hen watershed and are well within the subalpine zone. This densely vegetated region is considerably different than previous fSCA and grain size retrievals of the Sierra Nevada that predominantly fly in alpine regions (Nolin and Dozier 2000; Painter et al., 2003; Painter et al., 2013). For the most abundant snow scene the average AVIRIS fSCA is 0.4673 which emphasizes that our region of study is densely vegetated which will make the discrimination of snow and its grain size more difficult (Painter et al., 2003). We must also concede that our endmember library, specifically snow, is based on a theoretical derivation of clean snow with only solar zenith angle as the varying input parameter. These theoretical endmembers therefore do not account for varying azimuthal angles, topography, or dirty snow. It is also unknown how valuable additional spectral resolution is to resolving forest and snow fractions in complex topography. Current vegetation corrections involve assuming the fSCA is similar in sub-canopy as it is for snow in the open and have been shown to still be misrepresented (Rittger et al., 2013; Raleigh et al., 2013). Lidar and other sub-canopy distributed temperature sensing (DTS) measurements may provide solutions to accurate fSCA retrievals in vegetation.

Our varying grain size retrieval methods for pixels where NDSI > 0.9 produced substantially varied results. In the 2/24/15 scene both AVIRIS and CASI grain size

retrieval methods produced excellent results. However, in a similar low snow scene (5/18/16) we see a substantially higher mean/median differences from both methods, and both overestimating grain size (CASI overpredicting slightly more often than AVIRIS). However, in the abundant snow scene (3/24/16) we find that both AVIRIS and CASI underestimating grain size, with CASI getting closer to the true grain size. Similar to our previous discussion on varying grain size for the simulated MODSCAG and simulated EnMAP products, our densely vegetated scene may contribute to such varied results. Further analysis in alpine regions, ground validated areas, and snowier scenes will improve these comparisons. We suggest that the low snow scene (2/24/15) produced excellent results due to the majority of snow grain size retrievals reaching the upper limit of our endmember library (1100 μm) for both the spectral mixture analysis and varied grain size retrieval methods. Therefore the difference was nearly zero in all comparisons.

3.9 Conclusion

In order to remotely sense fSCA, both high spatial and high temporal resolution are needed for increasingly detailed hydrological, ecological, and climate inferences and modeling. That is why MODSCAG remains one of the best global and regional snow data products available due to the high 1-2 day temporal resolution. Yet, future satellite systems with improvements in spatial and spectral resolution will help refine snow properties. This work presents comparisons of simulated MODSCAG and simulated EnMAP fSCA and grain size retrieval products which shows significant improvements to fSCA retrievals especially in low snow. For low snow and densely vegetated study regions, we should expect EnMAP to improve total SCA calculations by $\sim$75%. MODSCAG appears to lose accuracy in low snow. We conclude that MODSCAG, in low snow, can not discriminate snow as well as EnMAP due to a limited spatial and spectral resolution and leads to underestimates of fSCA, particularly in a densely vegetated region. The current model, MODSCAG, even in a densely vegetated region, works well in abundant snow. Regardless of snow content,

EnMAP should improve accuracy of fSCA (RMSE) calculations by at least ∼25% over MODSCAG. Despite both simulated products maintaining high RMSE grain size values, likely related to dense vegetation discussed in Section 3.8, the very low median/mean difference of simulated EnMAP is substantially closer to the real grain size value than MODSCAG. MODSCAG appears to overestimate in low snow scenes and underestimate in abundant snow scenes while EnMAP remains normally distributed about the true grain size. When compared to the the full spectral resolution of the reflectance band feature that AVIRIS offers, the grain size produced by CASI wavelengths is only marginally different, even though the CASI method is spectrally limited in the 1030 nm ice absorption feature. Both methods are likely inadequate in densely vegetated scenes in combination with low spatial resolution, and we assert that grain size calculations made using the 1.03-1.06 μm ice absorption feature for limited CASI channels is reasonable in clean snow and likely within the $\pm 25\mu$m range if the scene is not densely vegetated (2/24/15 as the only case) (Painter et al., 2013; Painter et al., 2016). Further studies in alpine regions and ground validations are needed to confirm this.

The improvements that we should expect from EnMAP for fSCA and grain size retrievals in a subalpine regions are substantial, but it is also reassuring and impressive that a snow data product at a nominal ∼500 m spatial resolution and 7 bands spectral resolution is doing a good job when snow cover is high. Additional work might involve comparisons with concurrent true MODSCAG retrievals for validation of the simulated model. Additional field validation methods, especially in areas of concern (i.e. dirty snow and shaded regions) and subsequent adjustments to the model will improve robustness. It will also prove insightful to conduct these comparisons for the rest of the regions of the flight lines where snow is more homogeneous like alpine regions, and other regions besides the Sierra Nevada. We plan to release the model under an open source license on Matlab's File Exchange. Improvements to the algorithm and development will help enable varying unmixing applications.

3.10 Acknowledgements

AVIRIS data collection was provided in collaboration with Nevada NASA EPSCoR project #NNX14AN24A. Pipeline processing and correction of AVIRIS data was supported under NASA HyspIRI Preparatory Airborne Activities Grant NNX12AQ17G to the University of Nevada, Reno. Funding for this work also provided by Prof. Calvin's discretionary funds from the State of Nevada.

Appendix A

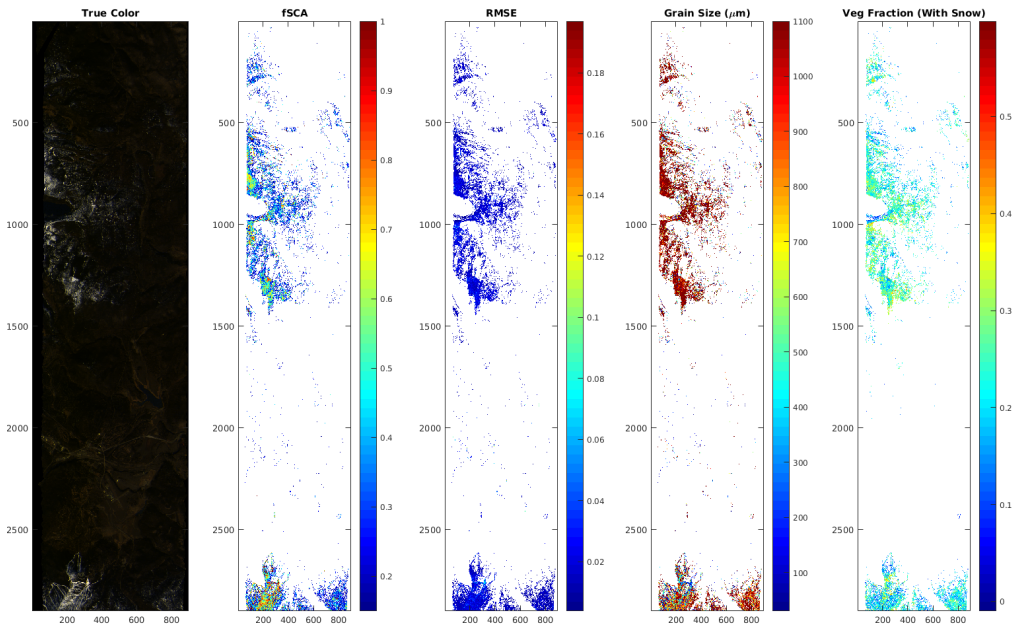

Figure A.1: AVIRIS flight line like **Figure 3.5**. Validation AVIRIS flight line from 2/24/15. This flight line is a low snow year.

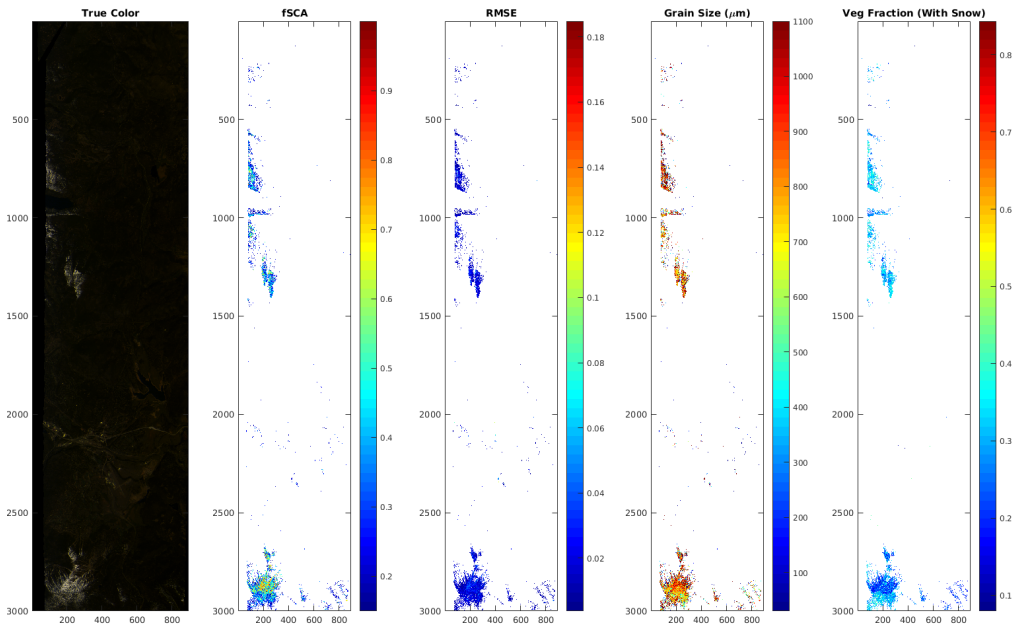

Figure A.2: AVIRIS flight line like **Figure 3.5**. Validation AVIRIS flight line from 5/18/16. This flight line represents snow ablation and snow loss.

References

Adams, J. B. (1993). Imaging spectroscopy: Interpretation based on spectral mixture analysis. *Remote geochemical analysis: Elemental and mineralogical composition*, pages 145–166.

Bair, E. H., Rittger, K., Davis, R. E., Painter, T. H., and Dozier, J. (2016). Validating reconstruction of snow water equivalent in California's Sierra Nevada using measurements from the NASA Airborne Snow Observatory. *Water Resources Research*, 52(11):8437–8460.

Baldridge, A., Hook, S., Grove, C., and Rivera, G. (2009). The ASTER spectral library version 2.0. *Remote Sensing of Environment*, 113(4):711–715.

Barnes, W. L., Pagano, T. S., and Salomonson, V. V. (1998). Prelaunch characteristics of the moderate resolution imaging spectroradiometer (MODIS) on EOS-AM1. *IEEE Transactions on Geoscience and Remote Sensing*, 36(4):1088–1100.

Calvin, W. M. and Hill, R. (2016). Imaging spectroscopy techniques for rapid assessment of geologic and cryospheric science data from future satellite sensors.

CaraDonna, P. J., Iler, A. M., and Inouye, D. W. (2014). Shifts in flowering phenology reshape a subalpine plant community. *Proceedings of the National Academy of Sciences*, 111(13):4916–4921.

Choler, P. (2005). Consistent shifts in alpine plant traits along a mesotopographical gradient. *Arctic, Antarctic, and Alpine Research*, 37(4):444–453.

Clark, M. P., Hendrikx, J., Slater, A. G., Kavetski, D., Anderson, B., Cullen, N. J., Kerr, T., Örn Hreinsson, E., and Woods, R. A. (2011). Representing spatial variability of snow water equivalent in hydrologic and land-surface models: A review. *Water Resources Research*, 47(7).

Clark, M. P., Slater, A. G., Barrett, A. P., Hay, L. E., McCabe, G. J., Rajagopalan, B., and Leavesley, G. H. (2006). Assimilation of snow covered area information into hydrologic and land-surface models. *Advances in water resources*, 29(8):1209–1221.

Coons, L. P., Nolin, A. W., Gleason, K. E., Mar, E. J., Rittger, K., Roth, T. R., and Painter, T. H. (2015). Seeing the snow through the trees. *Remote Sensing of the Terrestrial Water Cycle*, pages 199–213.

Cristea, N. C., Breckheimer, I., Raleigh, M. S., HilleRisLambers, J., and Lundquist, J. D. (2017). An evaluation of terrain-based downscaling of fractional snow covered area datasets based on lidar-derived snow data and orthoimagery. *Water Resources Research*.

Czyzowska-Wisniewski, E. H., van Leeuwen, W. J., Hirschboeck, K. K., Marsh, S. E., and Wisniewski, W. T. (2015). Fractional snow cover estimation in complex alpine-forested environments using an artificial neural network. *Remote Sensing of Environment*, 156:403–417.

Dedieu, J.-P., Carlson, B. Z., Bigot, S., Sirguey, P., Vionnet, V., and Choler, P. (2016). On the importance of high-resolution time series of optical imagery for quantifying the effects of snow cover duration on alpine plant habitat. *Remote Sensing*, 8(6):481.

Dozier, J. (1989). Spectral signature of alpine snow cover from the Landsat Thematic Mapper. *Remote sensing of environment*, 28:9–22.

Dozier, J., Green, R. O., Nolin, A. W., and Painter, T. H. (2009). Interpretation of snow properties from imaging spectrometry. *Remote Sensing of Environment*, 113:S25–S37.

Dozier, J., Painter, T. H., Rittger, K., and Frew, J. E. (2008). Time–space continuity of daily maps of fractional snow cover and albedo from MODIS. *Advances in Water Resources*, 31(11):1515–1526.

Finger, D., Pellicciotti, F., Konz, M., Rimkus, S., and Burlando, P. (2011). The value of glacier mass balance, satellite snow cover images, and hourly discharge for improving the performance of a physically based distributed hydrological model. *Water resources research*, 47(7).

Flanner, M. G., Zender, C. S., Hess, P. G., Mahowald, N. M., Painter, T. H., Ramanathan, V., and Rasch, P. (2009). Springtime warming and reduced snow cover from carbonaceous particles. *Atmospheric Chemistry and Physics*, 9(7):2481–2497.

Flanner, M. G., Zender, C. S., Randerson, J. T., and Rasch, P. J. (2007). Present-day climate forcing and response from black carbon in snow. *Journal of Geophysical Research: Atmospheres*, 112(D11).

Ford, K. R., Ettinger, A. K., Lundquist, J. D., Raleigh, M. S., and Lambers, J. H. R. (2013). Spatial heterogeneity in ecologically important climate variables at coarse and fine scales in a high-snow mountain landscape. *PloS one*, 8(6):e65008.

Franz, K. J. and Karsten, L. R. (2013). Calibration of a distributed snow model using MODIS snow covered area data. *Journal of hydrology*, 494:160–175.

Gao, B.-C., Heidebrecht, K. B., and Goetz, A. F. (1993). Derivation of scaled surface reflectances from AVIRIS data. *Remote sensing of Environment*, 44(2-3):165–178.

Gillespie, A. (1990). Interpretation of residual images: spectral mixture analysis of AVIRIS images, Owens Valley, California. In *Proc. second airborne visible/infrared imaging spectrometer (AVIRIS) workshop*, pages 243–270. Jet Propulsion Laboratory.

Green, R. O., Dozier, J., Roberts, D., and Painter, T. (2002). Spectral snow-reflectance models for grain-size and liquid-water fraction in melting snow for the solar-reflected spectrum. *Annals of Glaciology*, 34:71–73.

Green, R. O., Eastwood, M. L., Sarture, C. M., Chrien, T. G., Aronsson, M., Chippendale, B. J., Faust, J. A., Pavri, B. E., Chovit, C. J., Solis, M., et al. (1998). Imaging spectroscopy and the airborne visible/infrared imaging spectrometer (aviris). *Remote sensing of environment*, 65(3):227–248.

Green, R. O., Painter, T. H., Roberts, D. A., and Dozier, J. (2006). Measuring the expressed abundance of the three phases of water with an imaging spectrometer over melting snow. *Water Resources Research*, 42(10).

Guanter, L., Kaufmann, H., Segl, K., Foerster, S., Rogass, C., Chabrillat, S., Kuester, T., Hollstein, A., Rossner, G., Chlebek, C., et al. (2015). The EnMAP spaceborne imaging spectroscopy mission for earth observation. *Remote Sensing*, 7(7):8830–8857.

Hall, D., Chang, A., Foster, J., Benson, C., and Kovalick, W. (1989). Comparison of in situ and Landsat derived reflectance of Alaskan glaciers. *Remote Sensing of Environment*, 28:23–31.

Hall, D. K. and Riggs, G. A. (2007). Accuracy assessment of the MODIS snow products. *Hydrological processes*, 21(12):1534–1547.

Hill, R. G., Calvin, W. M., and Harpold, A. (2016). Subpixel Snow-covered Area Including Differentiated Grain Size from AVIRIS Data over the Sierra Nevada Mountain Range.

Justice, C. O., Román, M. O., Csiszar, I., Vermote, E. F., Wolfe, R. E., Hook, S. J., Friedl, M., Wang, Z., Schaaf, C. B., Miura, T., et al. (2013). Land and cryosphere products from Suomi NPP VIIRS: Overview and status. *Journal of Geophysical Research: Atmospheres*, 118(17):9753–9765.

Klein, A. G., Hall, D. K., Riggs, G. A., et al. (1998). Improving snow cover mapping in forests through the use of a canopy reflectance model. *Hydrological Processes*, 12(10):1723–1744.

Kokaly, R. F., Clark, R. N., Swayze, G. A., Livo, K. E., Hoefen, T. M., Pearson, N. C., Wise, R. A., Benzel, W. M., Lowers, H. A., Driscoll, R. L., et al. (2017). USGS spectral library version 7. Technical report, US Geological Survey.

Kunkel, K. E., Robinson, D. A., Champion, S., Yin, X., Estilow, T., and Frankson, R. M. (2016). Trends and extremes in Northern Hemisphere snow characteristics. *Current Climate Change Reports*, 2(2):65–73.

Lee, C. M., Cable, M. L., Hook, S. J., Green, R. O., Ustin, S. L., Mandl, D. J., and Middleton, E. M. (2015). An introduction to the NASA Hyperspectral InfraRed Imager (HyspIRI) mission and preparatory activities. *Remote Sensing of Environment*, 167:6–19.

Li, H. Y., He, Y. Q., Hao, X. H., Che, T., Wang, J., and Huang, X. D. (2015). Downscaling snow cover fraction data in mountainous regions based on simulated inhomogeneous snow ablation. *Remote Sensing*, 7(7):8995–9019.

Luce, C. H., Tarboton, D. G., and Cooley, K. R. (1999). Sub-grid parameterization of snow distribution for an energy and mass balance snow cover model. *Hydrological Processes*, 13(12):1921–1933.

Lundquist, J. D. and Dettinger, M. D. (2005). How snowpack heterogeneity affects diurnal streamflow timing. *Water Resources Research*, 41(5).

Matsunaga, T., Iwasaki, A., Tsuchida, S., Iwao, K., Tanii, J., Kashimura, O., Nakamura, R., Yamamoto, H., Kato, S., Mouri, K., et al. (2016). Current status of Hyperspectral Imager Suite (HISUI) and its deployment plan on International Space Station. In *Geoscience and Remote Sensing Symposium (IGARSS), 2016 IEEE International*, pages 257–260. IEEE.

McGuire, M., Wood, A. W., Hamlet, A. F., and Lettenmaier, D. P. (2006). Use of satellite data for streamflow and reservoir storage forecasts in the Snake River Basin. *Journal of Water Resources Planning and Management*, 132(2):97–110.

Nolin, A. W. (2010). Recent advances in remote sensing of seasonal snow. *Journal of Glaciology*, 56(200):1141–1150.

Nolin, A. W. and Daly, C. (2006). Mapping ''at risk'' snow in the Pacific Northwest. *Journal of Hydrometeorology*, 7(5):1164–1171.

Nolin, A. W. and Dozier, J. (1993). Estimating snow grain size using AVIRIS data. *Remote sensing of environment*, 44(2-3):231–238.

Nolin, A. W. and Dozier, J. (2000). A hyperspectral method for remotely sensing the grain size of snow. *Remote sensing of Environment*, 74(2):207–216.

Painter, T. H., Barrett, A. P., Landry, C. C., Neff, J. C., Cassidy, M. P., Lawrence, C. R., McBride, K. E., and Farmer, G. L. (2007). Impact of disturbed desert soils on duration of mountain snow cover. *Geophysical Research Letters*, 34(12).

Painter, T. H., Berisford, D. F., Boardman, J. W., Bormann, K. J., Deems, J. S., Gehrke, F., Hedrick, A., Joyce, M., Laidlaw, R., Marks, D., et al. (2016). The Airborne Snow Observatory: Fusion of scanning lidar, imaging spectrometer, and physically-based modeling for mapping snow water equivalent and snow albedo. *Remote Sensing of Environment*, 184:139–152.

Painter, T. H., Brodzik, M. J., Racoviteanu, A., and Armstrong, R. (2012). Automated mapping of Earth's annual minimum exposed snow and ice with MODIS. *Geophysical Research Letters*, 39(20).

Painter, T. H., Dozier, J., Roberts, D. A., Davis, R. E., and Green, R. O. (2003). Retrieval of subpixel snow-covered area and grain size from imaging spectrometer data. *Remote Sensing of Environment*, 85(1):64–77.

Painter, T. H., Rittger, K., McKenzie, C., Slaughter, P., Davis, R. E., and Dozier, J. (2009). Retrieval of subpixel snow covered area, grain size, and albedo from MODIS. *Remote Sensing of Environment*, 113(4):868–879.

Painter, T. H., Roberts, D. A., Green, R. O., and Dozier, J. (1998). The effect of grain size on spectral mixture analysis of snow-covered area from AVIRIS data. *Remote Sensing of Environment*, 65(3):320–332.

Painter, T. H., Seidel, F. C., Bryant, A. C., McKenzie Skiles, S., and Rittger, K. (2013). Imaging spectroscopy of albedo and radiative forcing by light-absorbing impurities in mountain snow. *Journal of Geophysical Research: Atmospheres*, 118(17):9511–9523.

Parajka, J. and Blöschl, G. (2008). The value of MODIS snow cover data in validating and calibrating conceptual hydrologic models. *Journal of Hydrology*, 358(3-4):240–258.

Raleigh, M. S., Rittger, K., Moore, C. E., Henn, B., Lutz, J. A., and Lundquist, J. D. (2013). Ground-based testing of MODIS fractional snow cover in subalpine meadows and forests of the Sierra Nevada. *Remote Sensing of Environment*, 128:44–57.

Rittger, K., Painter, T. H., and Dozier, J. (2013). Assessment of methods for mapping snow cover from MODIS. *Advances in Water Resources*, 51:367–380.

Rosenthal, W. and Dozier, J. (1996). Automated mapping of montane snow cover at subpixel resolution from the Landsat Thematic Mapper. *Water Resources Research*, 32(1):115–130.

Salomonson, V. V. and Appel, I. (2004). Estimating fractional snow cover from MODIS using the normalized difference snow index. *Remote sensing of environment*, 89(3):351–360.

Salomonson, V. V. and Appel, I. (2006). Development of the Aqua MODIS NDSI fractional snow cover algorithm and validation results. *IEEE Transactions on geoscience and remote sensing*, 44(7):1747–1756.

Skiles, S. M., Painter, T. H., Deems, J. S., Bryant, A. C., and Landry, C. C. (2012). Dust radiative forcing in snow of the Upper Colorado River Basin: 2. Interannual variability in radiative forcing and snowmelt rates. *Water Resources Research*, 48(7).

Stoelinga, M. T., Albright, M. D., and Mass, C. F. (2010). A new look at snowpack trends in the Cascade Mountains. *Journal of Climate*, 23(10):2473–2491.

Thirel, G., Salamon, P., Burek, P., and Kalas, M. (2011). Assimilation of MODIS snow cover area data in a distributed hydrological model. *Hydrology and Earth System Sciences Discussions*, (1):1329–1364.

Thompson, D. R., Gao, B.-C., Green, R. O., Roberts, D. A., Dennison, P. E., and Lundeen, S. R. (2015). Atmospheric correction for global mapping spectroscopy: ATREM advances for the HyspIRI preparatory campaign. *Remote Sensing of Environment*, 167:64–77.

Venn, S. E., Green, K., Pickering, C. M., and Morgan, J. W. (2011). Using plant functional traits to explain community composition across a strong environmental filter in Australian alpine snowpatches. *Plant Ecology*, 212(9):1491–1499.

Walters, R. D., Watson, K. A., Marshall, H.-P., McNamara, J. P., and Flores, A. N. (2014). A physiographic approach to downscaling fractional snow cover data in mountainous regions. *Remote sensing of environment*, 152:413–425.

Wang, X.-Y., Wang, J., Jiang, Z.-Y., Li, H.-Y., and Hao, X.-H. (2015). An effective method for snow-cover mapping of dense coniferous forests in the upper Heihe river basin using Landsat operational land imager data. *Remote Sensing*, 7(12):17246–17257.

Williams, R. S., Hall, D. K., and Benson, C. S. (1991). Analysis of glacier facies using satellite techniques. *Journal of Glaciology*, 37(125):120–128.

Wiscombe, W. J. and Warren, S. G. (1980). A model for the spectral albedo of snow. I: Pure snow. *Journal of the Atmospheric Sciences*, 37(12):2712–2733.